


BPL3 binds the long non-coding RNA *nalncFL7* to suppress *FORKED-LIKE7* and modulate HAI1-mediated MPK3/6 dephosphorylation in plant immunity

Gan Ai ,¹ Tianli Li ,¹ Hai Zhu ,¹ Xiaohua Dong ,¹ Xiaowei Fu ,¹ Chuyan Xia ,¹ Weiye Pan ,¹ Maofeng Jing ,¹ Danyu Shen ,¹ Ai Xia ,¹ Brett M. Tyler ² and Daolong Dou ^{1,*}

¹ College of Plant Protection, Academy for Advanced Interdisciplinary Studies, Nanjing Agricultural University, Nanjing 210095, China

² Center for Quantitative Life Sciences and Department of Botany and Plant Pathology, Oregon State University, Corvallis, Oregon 97331, USA

*Author for correspondence: ddou@njau.edu.cn

These authors contributed equally (G.A. and T.L.)

D.D. and G.A. designed the research. G.A., T.L., H.Z., X.D., X.F., C.X., and W.P. performed the research. G.A. and T.L. analyzed the data. D.D., T.L., G.A., M.J., D.S., A.X., and B.M.T. wrote the manuscript. All authors read and approved the final manuscript.

The author responsible for distribution of materials integral to the findings presented in this article in accordance with the policy described in the Instructions for Authors (<https://academic.oup.com/plcell>) is: Daolong Dou (ddou@njau.edu.cn).

Abstract

RNA-binding proteins (RBPs) participate in a diverse set of biological processes in plants, but their functions and underlying mechanisms in plant–pathogen interactions are largely unknown. We previously showed that *Arabidopsis thaliana* BPA1-LIKE PROTEIN3 (BPL3) belongs to a conserved plant RBP family and negatively regulates reactive oxygen species (ROS) accumulation and cell death under biotic stress. In this study, we demonstrate that BPL3 suppresses *FORKED-LIKE7* (*FL7*) transcript accumulation and raises levels of the cis-natural antisense long non-coding RNA (lncRNA) of *FL7* (*nalncFL7*). *FL7* positively regulated plant immunity to *Phytophthora capsici* while *nalncFL7* negatively regulated resistance. We also showed that BPL3 directly binds to and stabilizes *nalncFL7*. Moreover, *nalncFL7* suppressed accumulation of *FL7* transcripts. Furthermore, *FL7* interacted with HIGHLY ABA-INDUCED PP2C1 (HAI1), a type 2C protein phosphatase, and inhibited HAI1 phosphatase activity. By suppressing HAI1 activity, *FL7* increased the phosphorylation levels of MITOGEN-ACTIVATED PROTEIN KINASE 3 (MPK3) and MPK6, thus enhancing immunity responses. BPL3 and *FL7* are conserved in all plant species tested, but the BPL3–*nalncFL7*–*FL7* cascade was specific to the Brassicaceae. Thus, we identified a conserved BPL3–*nalncFL7*–*FL7* cascade that coordinates plant immunity.

Introduction

RNA-binding proteins (RBPs) are a diverse class of proteins defined by their ability to interact with RNA molecules. In *Arabidopsis* (*Arabidopsis thaliana*), more than 800 RBPs have been identified (Lorkovic and Barta, 2002). One of the most-abundant RNA-binding domains is the RNA-recognition motif (RRM), present in 197 *Arabidopsis* proteins (Silverman et al, 2013). RRM proteins are involved in pre-mRNA splicing RNA

stability, and editing (Duque, 2011). They affect nearly all stages of the life cycle as they contribute to seed germination and development, plant growth, and responses to biotic and abiotic stress (Ma et al, 2021). For example, the RNA binding protein RBP-P binds to both glutelin and prolamine mRNAs, regulating their RNA metabolism and eventually grain development in rice (*Oryza sativa*) (Tian et al, 2018). PigmR-

IN A NUTSHELL

Background: RNA-binding proteins (RBPs) are a diverse class of proteins defined by their ability to interact with RNA molecules. They affect nearly all stages of the plant life cycle as they contribute to seed germination and development, plant growth, and responses to stress. Nevertheless, the role of RBPs in plant–pathogen interactions is still largely unknown. We previously reported that the RBPs BPA1-like proteins (BPLs) are conserved negative regulators of plant immunity. Among these, BPL3 makes a major non-redundant contribution to this function.

Question: What is the underlying mechanism by which BPL3 regulates plant immunity?

Findings: We demonstrated that BPL3 regulates the transcript level of a natural pair of sense and anti-sense transcripts, *FL7* (*FORKED-LIKE 7*) and its cis-natural antisense lncRNA of *FL7* (*nalncFL7*). *nalncFL7* suppresses *FL7* at the transcriptional level and BPL3 binds to and stabilizes *nalncFL7*. *FL7* interacts with the type 2C protein phosphatase HIGHLY ABA-INDUCED PP2C1 (*HAI1*). By suppressing *HAI1* phosphatase activity, *FL7* promotes phosphorylation of the kinases MPK3 and MPK6, and thus enhances immune responses. BPL3 and *FL7* were conserved in all the tested plants, but the BPL3–*nalncFL7*–*FL7* cascade was found in Brassicaceae plants. Thus, our study identified a conserved BPL3–*nalncFL7*–*FL7* cascade that acts in plant immunity.

Next steps: We found that BPL3 and *FL7* are conserved in land plants while *nalncFL7* was conserved in Brassicaceae, which indicates that the BPL3–*nalncFL7*–*FL7* cascade might have arisen after the divergence of Brassicaceae species. Whether and how BPL3 could regulate *FL7* outside of the Brassicaceae remains unknown.

INTERACTING and BLAST RESISTANCE PROTEIN 1 (PIBP1), an RRM-containing protein in rice, interacts with the resistance protein PigmR (Pigm Resistant) and translocates to the nucleus to activate the expression of defense-related genes and ensure full resistance against rice blast (Zhai et al., 2019). Nevertheless, the role of RRM proteins in plant–pathogen interactions is still largely unclear.

Long non-coding RNAs (lncRNAs) are RNAs produced by a mechanism other than a molecular ruler-based dicing or trimming and function independently of their protein-coding potential (Wierzbicki et al., 2021). With the advent of high-throughput sequencing, thousands of lncRNAs have been identified in multiple plant species such as rice (Zhang et al., 2014) and *A. thaliana* (Di et al., 2014). Plant lncRNAs play important roles in development, RNA processing, and in biotic and abiotic stress responses (Wierzbicki et al., 2021). In the context of plant–pathogen interactions, few lncRNAs have been reported to be vital regulators. The Arabidopsis lncRNA *ELENA1* is a positive regulator that enhances resistance to *Pseudomonas syringae* pv. *tomato* DC3000 by elevating *PATHOGENESIS-RELATED1* (*PR1*) expression (Seo et al., 2017, 2019). In tomato (*Solanum lycopersicum*), the lncRNA *Slylnc0195* appears to modulate genes encoding class III homeodomain-leucine zipper (HD-Zip)-type transcription factors by acting as target mimic for microRNA166 (miR166) during tomato responses to tomato yellow leaf curl virus (TYLCV) (Wang et al., 2015). Also in tomato, *lncRNA16397* induced the expression of glutaredoxin (*GRX*) genes and enhanced tomato resistance against the fungus *Phytophthora infestans* (Cui et al., 2017). Interestingly, we recently showed that TYLCV viral sRNAs and host lncRNAs together could support the development of disease phenotypes and host antiviral immunity (Yang et al., 2019).

lncRNAs are commonly classified according to their location and orientation relative to neighboring protein-coding transcripts (Liu et al., 2015). Some lncRNAs generated from natural antisense transcripts (NATs) are called *nalncRNAs*. NATs may initiate on the reverse strand of sense protein-coding regions (cis-NATs) or may be complementary to a sense transcript originating from a distal genomic locus (trans-NATs) (Bouchard et al., 2015). Studies have revealed that cis-NATs can participate in a broad range of regulatory events (Lapidot and Pilpel, 2006), including small interfering RNA (siRNA)-induced gene silencing (Borsani et al., 2005; Katiyar-Agarwal et al., 2006; Li et al., 2020). For example, a cis-NAT in Arabidopsis, *SIMILAR TO RCD-ONE 5* (*SRO5*), is induced by salt and produces small RNAs to suppress the accumulation of its complementary transcript, *DELTA(1)-PYRROLINE-5-CARBOXYLATE DEHYDROGENASE* (*P5CDH*), to regulate plant salt resistance (Borsani et al., 2005). Another cis-NAT, *RAB2-LIKE SMALL GTP-BINDING PROTEIN2* (*ATGB2*), contributes to race-specific disease resistance by repressing *PENTATRICOPEPTIDE REPEATS PROTEIN-LIKE* (*PPRL*) through a small RNA-dependent pathway (Katiyar-Agarwal et al., 2006). Even though these cis-NATs are known to take part in plant responses to biotic and abiotic stresses (Borsani et al., 2005), the role of other cis-NATs in pathogen–host interactions remains unexplored.

A MITOGEN-ACTIVATED PROTEIN KINASE (MAPK) is activated when phosphorylated at its activation loop by a dual specificity kinase (MAPKK, MAPK KINASE) (Zhang et al., 2018a). Such activities of MAPKs are regulated by a large family of protein serine/threonine phosphatases (PSPs) by dephosphorylation (Schweighofer et al., 2004), including type 2C protein phosphatases (PP2Cs) (Schweighofer et al., 2004; Singh et al., 2016). The Arabidopsis genome encodes 80 PP2Cs that are subdivided into 12 groups (A–K)

(Schweighofer et al., 2004; Fuchs et al., 2013). The type B PP2C, AtAP2C1, was reported to interact with and inactivate AtMAPK4/6 via dephosphorylation to regulate jasmonic acid (JA) and ethylene biosynthesis, thus modulating innate immunity (Schweighofer et al., 2007). In addition, type A PP2Cs also deactivate MAPKs. For example, the redundant Arabidopsis PP2Cs HIGHLY ABA-INDUCED PP2C1 (HAI1), HAI2, and HAI3 interact with and dephosphorylate MPK3 and MPK6 to suppress immunity against biotrophic and hemibiotrophic pathogens (Mine et al., 2017).

PP2C family proteins do not have regulatory subunits, which is distinct from other phosphoprotein phosphatases (Shi, 2009; Lillo et al., 2014). The phosphatase activity of PP2CA proteins is inhibited via specific interactions with the small abscisic acid (ABA) receptors including PYRABACTIN RESISTANCE1 (PYR1), PYR1-LIKE (PYLs), and REGULATORY COMPONENT OF ABA RECEPTORS (RCARs) (Park et al., 2009; Tischer et al., 2017). After binding to ABA, PYR1/PYLs/RCARs interact with and inhibit PP2CAs, resulting in the activation of downstream protein kinases (Fujii et al., 2009; Park et al., 2009). In the absence of ABA, several PYR1/PYLs/RCARs can still interact with and inhibit PP2CAs (Hao et al., 2011). It is worthwhile to investigate whether other proteins may hinder the phosphatase activity of PP2CA proteins.

We have previously reported that the BPL family of proteins, including BINDING PARTNER OF ACD11 (BPA1) and BPA1-LIKE PROTEINs (BPLs), are conserved negative regulators of plant immunity in Arabidopsis (Li et al., 2019; Zhang et al., 2020). Among these, BPL3 exhibited a distinct role as only *bpl3* single mutants showed higher resistance levels against *Phytophthora capsici*, while other BPL proteins appeared to be functionally redundant in modulating resistance to *P. capsici* (Li et al., 2019). Here, we identified FL7 (FORKED-LIKE7) and its natural antisense lncRNA, *nalncFL7*. We demonstrate that BPL3 can directly bind to and stabilize *nalncFL7*, which subsequently suppresses the accumulation of FL7 transcripts. Furthermore, FL7 associated with and suppressed the activity of a PP2CA protein, HAI1, leading to lower phosphorylation levels of MPK3 and MPK6. Thus, we identified a signaling cascade consisting of BPL3, *nalncFL7* and FL7 that modulates MAPK phosphorylation and plant immunity.

Results

BPL3 negatively regulates plant immunity

To validate that BPL3 is a negative regulator of plant immunity (Li et al., 2019), we generated *gBPL3-FLAG* complementation lines by transforming a BPL3 genomic fragment driven by its native promoter into the *bpl3* background (Supplemental Figure S1A). The complementation lines (*bpl3 gBPL3*) showed BPL3 transcript levels comparable to those of the wild type. Another line (*bpl3 OE-BPL3*) exhibited ~12-fold higher BPL3 transcript levels and was considered an overexpression line (Supplemental Figure S1B). We also confirmed BPL3 protein accumulation by immunoblotting with an anti-flag antibody (Supplemental Figure S1C).

The *bpl3 gBPL3* line fully eliminated the greater resistance of *bpl3* against *P. capsici* and *Pseudomonas syringae* DC3000 (Supplemental Figure S2, A–D), while overexpression in the *bpl3 OE-BPL3* line impaired resistance (Supplemental Figure S2, A–D), supporting the notion that BPL3 is a negative regulator of plant immunity.

When challenged by *P. capsici* zoospores, the *bpl3* mutant showed increased H₂O₂ accumulation, the complementation line had normal levels, and the overexpression line displayed lower H₂O₂ accumulation (Supplemental Figure S2E), which is consistent with our previous findings that BPL family proteins may negatively regulate reactive oxygen species (ROS) accumulation (Li et al., 2019). Furthermore, BPL3 negatively regulated the transcript levels of the well-characterized plant immunity marker gene *FLG22-INDUCED RECEPTOR-LIKE KINASE 1* (*FRK1*) (Breen et al., 2017) in response to *P. capsici* invasion (Supplemental Figure 2F). Based on our previously reported RNA-seq data of the *bpl3* mutant and wild type (Li et al., 2019), we identified 3,570 differentially expressed genes (DEGs) in the *bpl3* mutant, consisting of 2,637 upregulated and 933 downregulated genes in the mutant relative to the wild type (Supplemental Data Set S1). Gene Ontology (GO) analysis of the upregulated genes revealed immunity-related GO terms including “GO:0050896 response to stimulus,” “GO:0002376 immune system,” “GO:0023052 signaling,” and “GO:0001906 cell killing,” as being significantly enriched (Supplemental Figure S3). These results suggest that BPL3 negatively regulates plant resistance by inhibiting plant ROS accumulation and defense-related gene expression.

BPL3 regulates the abundance of a natural pair of sense and antisense transcripts

As BPL3 contains an RNA-binding motif, it may potentially regulate RNA alternative splicing or processing (Lorkovic, 2009; de Longevialle et al., 2010). Indeed, level-3 GO terms enriched in *bpl3* included multiple RNA processing-related terms (Supplemental Figure S4). Furthermore, the transcript of 1,540 genes showed potential splicing changes in *bpl3* compared with the wild type (Supplemental Data Set S2). The most significant change occurred at the At4g16670 locus, encoding FORKED-LIKE 7 (FL7) (Supplemental Data Set S2).

Further analysis indicated that the transcript changes involving FL7 do not result from alternative splicing events but rather from a differentially accumulated natural pair of sense and antisense transcripts. Indeed, an antisense transcript of FL7 (At4g06410, hereafter *nalncFL7*), had been annotated as a lncRNA that overlapped with exons 2–7 of the FL7 locus. The sense transcript of FL7 was hardly detected in Col-0, while *nalncFL7* strongly accumulated (Figure 1A). We confirmed the same phenomenon in two additional publicly available RNA-seq datasets from Col-0 (Supplemental Figure S5; Downen et al., 2012; Harris et al., 2018). By contrast, FL7 transcripts were dominant and *nalncFL7* transcripts were significantly less abundant in *bpl3* but not in *bpa1* or *bpl2* mutants (Figure 1A), which was further supported by reverse transcription PCR (RT-PCR) assays (Figure 1B).

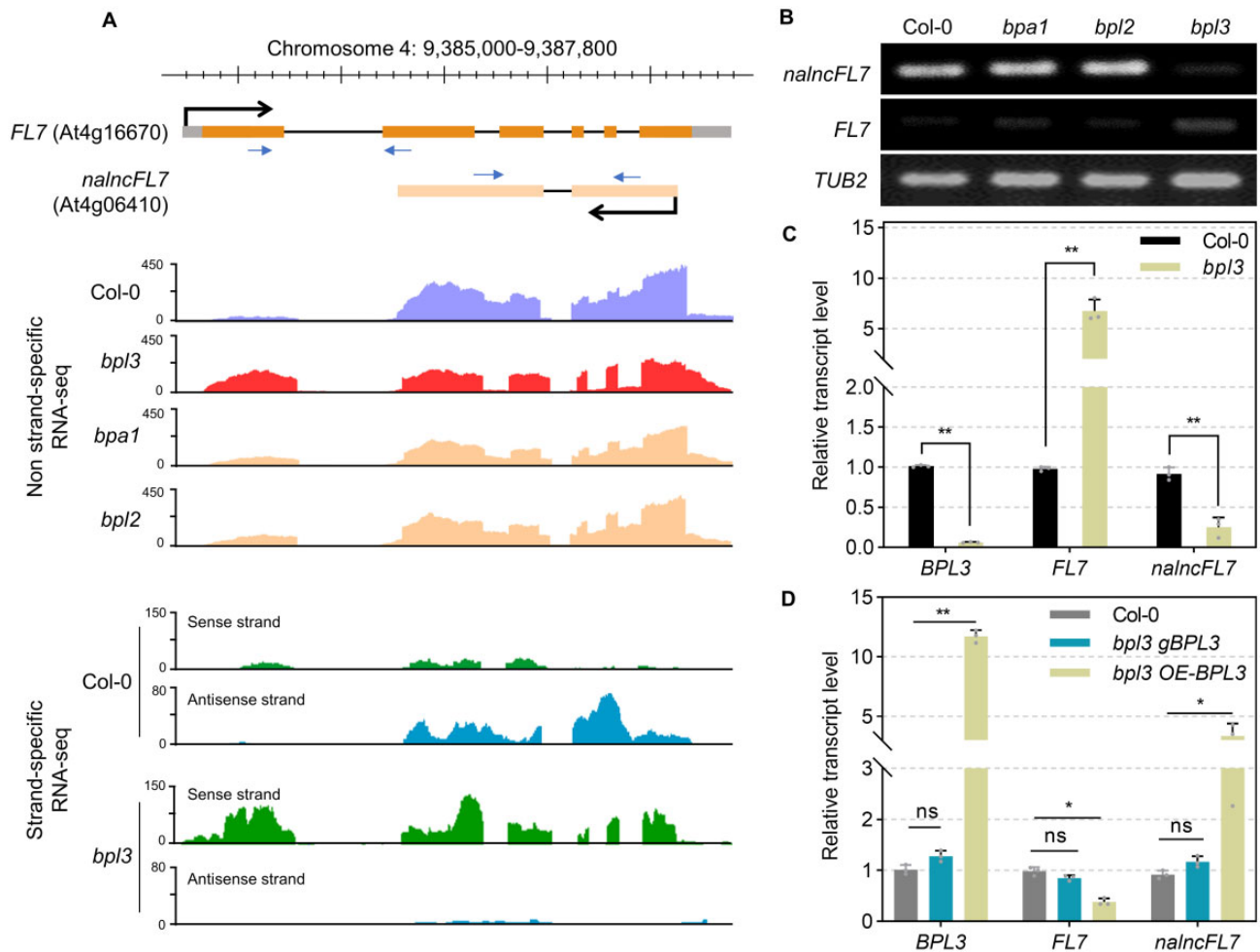


Figure 1 BPL3 regulates transcript abundance of *FL7* and *nalncFL7*. **A**, Transcript abundance of *FL7* and *nalncFL7*. Genome coordinates of *FL7* and *nalncFL7* are shown in the upper panel. Transcription direction is shown by arrows. RNA-seq data of the indicated plant genotypes were mapped to the Arabidopsis genome. Genome browser views of RNA-seq signals at *FL7* and *nalncFL7* in Col-0, with normalized read counts per million along the y-axis, are shown in the middle panel (non-strand-specific RNA-seq data) and lower panel (strand-specific RNA-seq data). **B**, Transcript levels of *FL7* and *nalncFL7* in the *bpl3* mutant detected by RT-PCR. RNA from indicated plants was extracted and assayed by RT-PCR. *AtTUB2* was used as the reference transcript. The position of primers is shown in (A). Experiments were performed three times with similar results. **C** and **D**, Relative transcript levels of *FL7* and *nalncFL7* in the *bpl3* mutant and over-expression plants, as assayed by RT-qPCR analysis. The *UBQ10* gene was used as reference transcript. Data are means \pm SD of three biological replicates ($n = 3$; * $P < 0.05$, ** $P < 0.01$, Student's *t* test, ns = not significant).

Moreover, we generated a strand-specific RNA-seq dataset in Col-0 and *bpl3*. The accumulation of *nalncFL7* was greatly inhibited in *bpl3*, while that of *FL7* increased in *bpl3*, compared with wild-type plants (Figure 1A). Most of the transcripts detected in the locus in Col-0 were *nalncFL7*, as determined by RT-quantitative PCR (RT-qPCR), in contrast to the *bpl3* mutant that had few *nalncFL7* transcripts and high levels of *FL7* mRNAs (Figure 1C). These results indicated that BPL3 facilitates the accumulation of *nalncFL7* but negatively regulates *FL7* transcript abundance. We obtained further support of this conclusion by analyzing *FL7* and *nalncFL7* transcript levels in the *bpl3* gBPL3 and *bpl3* OE-BPL3 lines (Figure 1D).

FL7 belongs to the *FL* gene family. We thus analyzed the antisense transcripts of the other eight members of this gene family (Supplemental Figure S6A). We detected

antisense transcripts for *FKD1* (*FORKED1*) and *FL8*; the antisense transcript of *FL8* was annotated as *At5g57760* encoding a hypothetical protein (Supplemental Figure S6B). To test whether BPL3 regulates *FL7* specifically, we measured the differences in transcript levels for the other eight *FL* members in the *bpl3* and *bpl3* OE-BPL3 lines (Supplemental Figure S7). We failed to detect *FL8* transcripts. We observed an increase in the transcript levels of *FL3* and *FL5* (50%–70%) in the *bpl3* mutant and a decrease (by 30%–60%) in the BPL3-overexpression line. *FL6* transcript levels decreased (by 80%) in the *bpl3* mutant and increased (by 80%) in the BPL3-overexpression line. *FL2* transcript levels were not significantly different across the tested genotypes. Other *FL*s exhibited expression alterations only in the *bpl3* mutant or the BPL3-overexpression line (Supplemental Figure S7). Based on these results, we conclude that several *FL*

members, including *FL3/5/6/7*, are regulated by BPL3. As *FL7* showed the most significant regulation by BPL3, we focused on *FL7* and *nalncFL7* in this study.

FL7 is a positive regulator of plant immunity

Whether *FL7* is involved in plant immunity is unknown, prompting us to investigate this possibility with an Arabidopsis mutant (*fl7*; SALK_077717) containing a T-DNA insertion in the first exon of *FL7* (Supplemental Figure S8A). *FL7* mRNA was almost undetectable in the T-DNA insertion mutant, however levels of *nalncFL7* were unaffected (Supplemental Figure S8B). We evaluated disease resistance phenotypes in the *fl7* mutant and Col-0 plants following inoculation with *P. capsici*. Assessment of the infected leaves at 36-h post inoculation (hpi) revealed significantly larger lesions on *fl7* leaves than on Col-0 leaves (Figure 2, A and B). Importantly, complementation of the *fl7* mutant with a genomic *FL7* fragment from its native promoter (Supplemental Figure S8, C and D) restored the wild-type phenotype, while overexpression of *FL7* under the control of the *Mannopine synthase* (*MAS*) promoter (Supplemental Figure S8, C and D) significantly increased plant resistance (Figure 2, A and B). Staining assays with 3,3'-diaminobenzidine (DAB) and RT-qPCR assays also suggested that the positive regulation of resistance by *FL7* is associated with increased plant ROS accumulation and *FRK1* expression (Figure 2, C and D). Taken together, we hypothesized that *FL7* is a positive regulator of plant immunity against *P. capsici*.

The results above led us to speculate that the increase of *FL7* transcript levels in *bpl3* is responsible for the enhanced disease resistance observed in *bpl3*. To test this possibility, we generated *fl7 bpl3* double mutant lines by crossing the *fl7* mutant with *bpl3*, and then evaluated its disease resistance. The *fl7 bpl3* double mutant showed comparable lesion sizes with the *fl7* single mutant (Figure 2, A and B), indicating that the *bpl3* allele cannot rescue the disease susceptibility phenotype of *fl7*. We also detected low levels of H₂O₂ and *FRK1* transcripts in *fl7* and *fl7 bpl3* leaves upon *P. capsici* inoculation (Figure 2, C and D). Thus, we conclude that BPL3-mediated plant immunity is mainly dependent on *FL7*.

nalncFL7 is a negative regulator of plant immunity

To investigate the role of *nalncFL7* in regulating plant immunity, we constructed *nalncFL7* overexpression lines (Supplemental Figure S8, C and E). *OE-nalncFL7* lines showed decreased resistance to *P. capsici* (Figure 2, E and F), impaired plant ROS accumulation (Figure 2G), and reduced *FRK1* expression (Figure 2H). We also obtained two *nalncFL7*-knockdown lines (*ami-nalncFL7-1* and *ami-nalncFL7-2*) by introducing two different artificial microRNAs (*amiR*) targeting *nalncFL7* into Arabidopsis (Supplemental Figure S8, A, C, and E). Both lines showed higher resistance to *P. capsici* (Figure 2, E and F), more plant ROS accumulation (Figure 2G), and higher *FRK1* transcript levels compared with the wild type (Figure 2H). These

results suggest that *nalncFL7* negatively regulates plant immunity.

BPL3 directly interacts with and stabilizes nalncFL7 transcripts

BPL3 contains an RNA-binding motif at its N terminus (amino acids [aa] 1–74). To test whether BPL3 interacts with *FL7* or *nalncFL7* transcripts, we performed in vitro RNA binding assays with 6XHis-tagged recombinant BPL3 protein and biotin-labeled *FL7* mRNA or *nalncFL7* RNA. We established that BPL3 associates with *nalncFL7* but not *FL7* in vitro (Figure 3A). Furthermore, binding competition assays with non-biotinylated RNA confirmed that *nalncFL7* specifically binds to BPL3 (Figure 3B). Electrophoretic mobility shift assay (EMSA) and competition assays also demonstrated that *nalncFL7* but not *FL7* interacts with BPL3 (Figure 3C). A BPL3 variant lacking the RRM domain, BPL3^{ΔRRM} (aa 75–244), failed to interact with *nalncFL7* RNA (Figure 3A), indicating that BPL3 has *nalncFL7*-binding activity through its RRM domain.

RBPs may regulate the stability of their target RNAs (Faghihi et al., 2008). Based on an RNA decay assay, we indeed observed that the stability of *nalncFL7* decreases in the *bpl3* mutant but increases in *bpl3 OE-BPL3* line (Figure 3D). By contrast, *FL7* transcripts degraded quickly in the *bpl3 OE-BPL3* line but were more stable in the *bpl3* mutant (Figure 3D). These results demonstrate that BPL3 positively regulates *nalncFL7* levels and negatively regulates *FL7* levels.

nalncFL7 suppresses FL7 accumulation

As BPL3 interacted with *nalncFL7* but not *FL7* transcripts, we next investigated how BPL3 regulates *FL7*. When we tested the changes in transcript levels of *nalncFL7* and *FL7* in different tissues, we noticed that their abundances are inversely correlated. *FL7* transcript levels were higher in roots and stems compared with leaf tissues, while transcript levels of *nalncFL7* were downregulated in roots, flowers, and siliques compared with leaf tissues (Supplemental Figure S9A). Therefore, we investigated whether *nalncFL7* might inhibit the transcript abundance of *FL7* by overexpressing *nalncFL7* in Arabidopsis protoplasts. Notably, overexpression of *nalncFL7* significantly decreased *FL7* transcript abundance compared with the empty vector control (Figure 4A). Interestingly, deleting the region over which *FL7* and *nalncFL7* overlap in an *FL7* variant construct abolished this inhibition by *nalncFL7* (Figure 4A). *FL7* accumulation was also impaired in *OE-nalncFL7* lines and rose in the *ami-nalncFL7-1* and *ami-nalncFL7-2* lines (Figure 4B). When we ectopically expressed *FL7* together with *nalncFL7* or an empty vector in *Nicotiana benthamiana* leaves, we observed that *nalncFL7* also suppresses *FL7* transcript accumulation in *N. benthamiana* (Figure 4, C–E). To exclude the possibility that unknown proteins encoded by *nalncFL7* may interfere with *FL7* abundance, we identified five potential open-reading frames (ORFs) in *nalncFL7* (Supplemental Figure S9B). We mutated all the start codons of these ORFs in *nalncFL7* to “CTG” (*nalncFL7_5M*) (Supplemental Figure

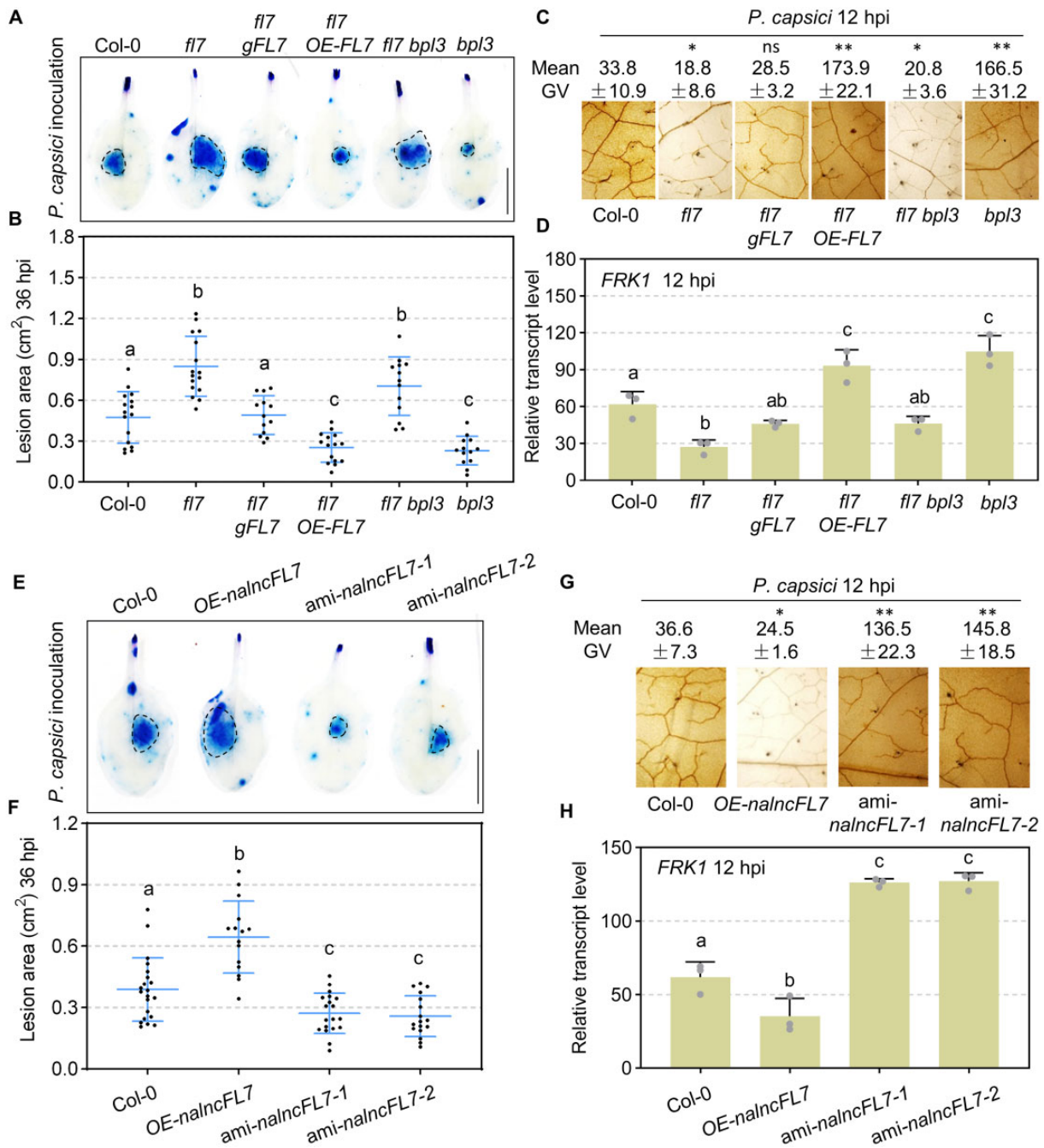


Figure 2 The role of *FL7* and *nalncFL7* in plant immunity. A and B, *Phytophthora capsici* inoculation phenotypes. Leaves of the indicated genotypes were detached and 400–500 *P. capsici* zoospores were placed in a droplet at the center of each leaf, and then incubated in a growth room at 25°C in darkness. Leaves were stained by trypan blue at 36 hpi (A). *Phytophthora capsici* lesion areas were measured in ImageJ and shown in (B). Data are means \pm SD of three biological replicates ($n > 12$; lowercase letters indicate significant differences tested between multiple groups by one-way ANOVA at $P < 0.05$). C, H₂O₂ detection. *Phytophthora capsici*-inoculated leaves were stained at 12 hpi with DAB for 8 h, then decolorized with ethanol, and photographed under light microscopy. Mean gray values from DAB staining results from six randomly chosen regions of infiltrated leaves are shown above. Data are means \pm SD of two biological replicates ($n = 6$; * $P < 0.05$, ** $P < 0.01$, Student's t test). D, Relative transcript levels of *FRK1*. Data are means \pm SD of three biological replicates ($n = 3$, lowercase letters indicate significant differences tested between multiple groups by one-way ANOVA at $P < 0.05$). E and F, *Phytophthora capsici* inoculation phenotypes. The indicated Arabidopsis leaves were treated as in (A and B). Data are means \pm SD of three biological replicates ($n > 14$; lowercase letters indicate significant differences tested between multiple groups by one-way ANOVA at $P < 0.05$). G, H₂O₂ detection. The indicated Arabidopsis leaves were treated as in (C). Data are means \pm SD of two biological replicates ($n = 6$; * $P < 0.05$, ** $P < 0.01$, Student's t test, ns = not significant). H, Relative *FRK1* transcript levels. Data are means \pm SD of three biological replicates ($n = 3$, lowercase letters indicate significant differences between multiple groups by one-way ANOVA at $P < 0.05$). For each experiment, several complementation or overexpression lines were used and one representative result is shown.

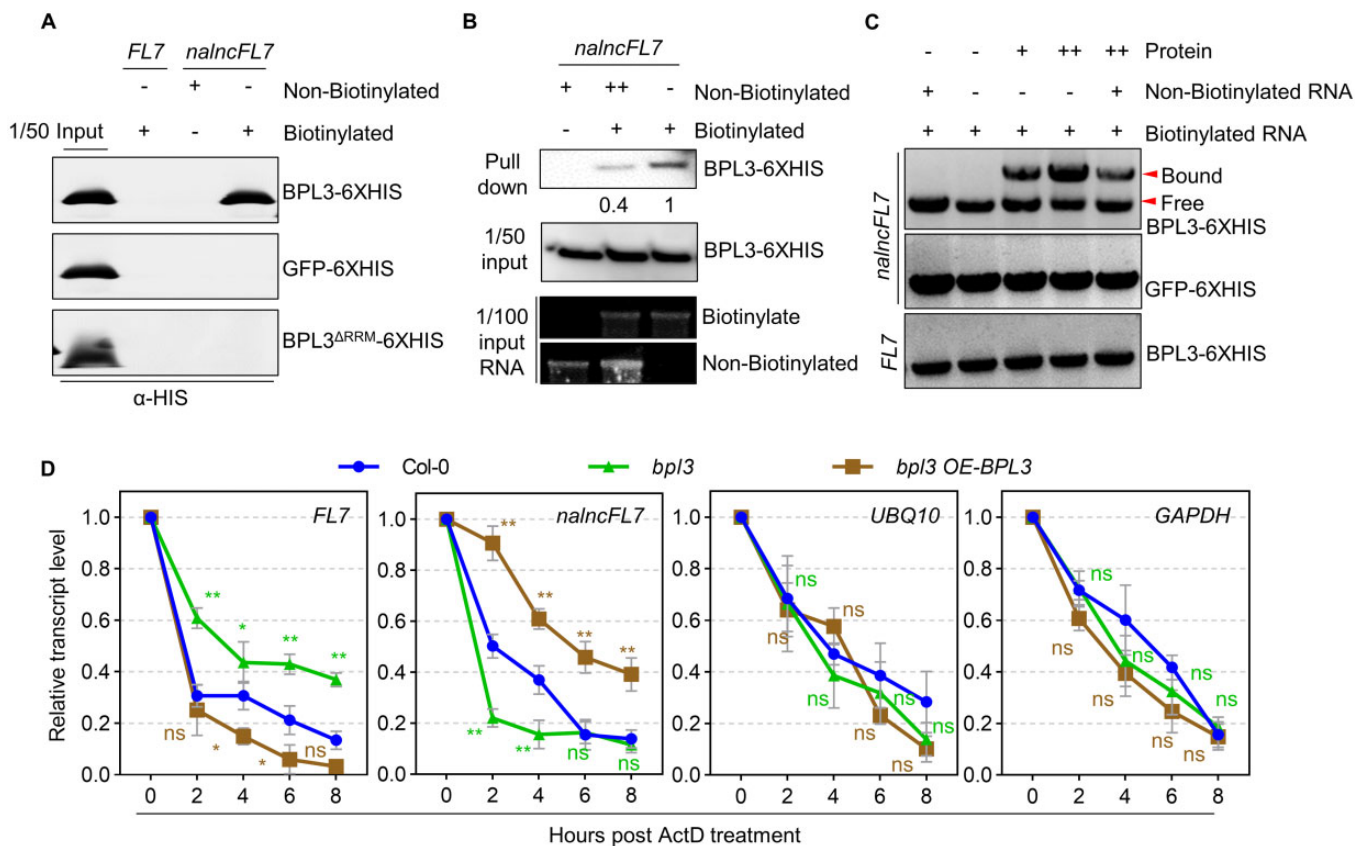


Figure 3 BPL3 directly interacts with and stabilizes *nalncFL7* transcripts. A, In vitro binding assay of BPL3 with *FL7* or *nalncFL7* RNAs. *FL7* and *nalncFL7* RNAs were in vitro-transcribed and biotinylated, and then incubated with recombinant GFP-6XHIS, BPL3-6XHIS, or BPL3^{ΔRRM}-6XHIS proteins, followed by biotinylated RNA pull-down. Immunoblotting results of the precipitates using an anti-HIS antibody are shown. Experiments were performed three times with similar results. B, In vitro binding competition assay with BPL3 and *nalncFL7* RNA. Non-biotinylated *nalncFL7* was used as a competitor to bind to BPL3; + and ++ indicate 2 and 10 mg of RNA, respectively. Experiments were performed three times with similar results. C, In vitro binding between BPL3 and *FL7* or *nalncFL7* RNA by RNA EMSA. The indicated biotinylated RNA was incubated with the indicated proteins (–, +, and ++ indicate 0, 0.5, or 2 μg of protein). The reaction mixtures were separated by electrophoresis on 1% (w/v) agarose gels in 0.5 × Tris-borate EDTA (TBE). The gel was electroblotted onto a nylon membrane. Experiments were performed three times with similar results. D, Stability of *FL7* and *nalncFL7* transcripts. Relative RNA levels were measured by RT-qPCR at different time points after treatment with the transcription inhibitor Act D (100 μg/mL) in wild type, *bpl3*, and *bpl3* OE-BPL3 lines. *UBQ10* and *GAPDH* were used as controls. Data are means ± SD of three technical replicates ($n = 3$; * $P < 0.05$, ** $P < 0.01$, two-way ANOVA, ns = not significant).

S9B), but this mutant transcript still prevented the accumulation of *FL7* transcripts (Supplemental Figure S9B), indicating that the function of *nalncFL7* is not dependent on any protein coding ability. Together, these results suggest that *nalncFL7* suppresses *FL7* in a trans rather than cis manner.

FL7 interacts with PP2C protein HAI1

Next, we investigated possible mechanisms by which FL7 might regulate plant immunity by identifying its interactors. Using the BioGRID database (<https://thebiogrid.org/>), we selected 16 putative interactors of FL7 (Supplemental Figure S10). One such candidate was a PP2C family protein, HAI1, which is involved in dephosphorylating and negatively regulating the MAPK cascade proteins MPK3 and MPK6 (Mine et al., 2017). We confirmed that FL7 interacts with HAI1 in vivo and in vitro via split-luciferase assays, co-immunoprecipitation (Co-IP), yeast two-hybrid (Y2H), and pull-down assays (Figure 5, A–D). To identify the functional

domains responsible for the interaction between FL7 and HAI1, we tested truncated versions of both proteins in Y2H assays (Figure 5C). We determined that the auxin canalization domain of FL7 and the phosphatase domain of HAI1 are necessary and sufficient for their interaction (Figure 5C). Pull-down assays further supported the idea that FL7 associates with the phosphatase domain of HAI1 in vitro (Figure 5D). We also tested the interaction between FL7 and HAI1 homolog proteins and observed that FL7 also interacts with HAI2 and HAI3 (Figure 5A).

FL7 directly inhibits the phosphatase activity of HAI1

That FL7 interacted with the phosphatase domain of HAI1 suggested that it might potentially inhibit the phosphatase activity of HAI1. To test this idea, we measured HAI1 phosphatase activity in the presence of FL7 in vitro. Recombinant HAI1 showed a significant inhibition of its

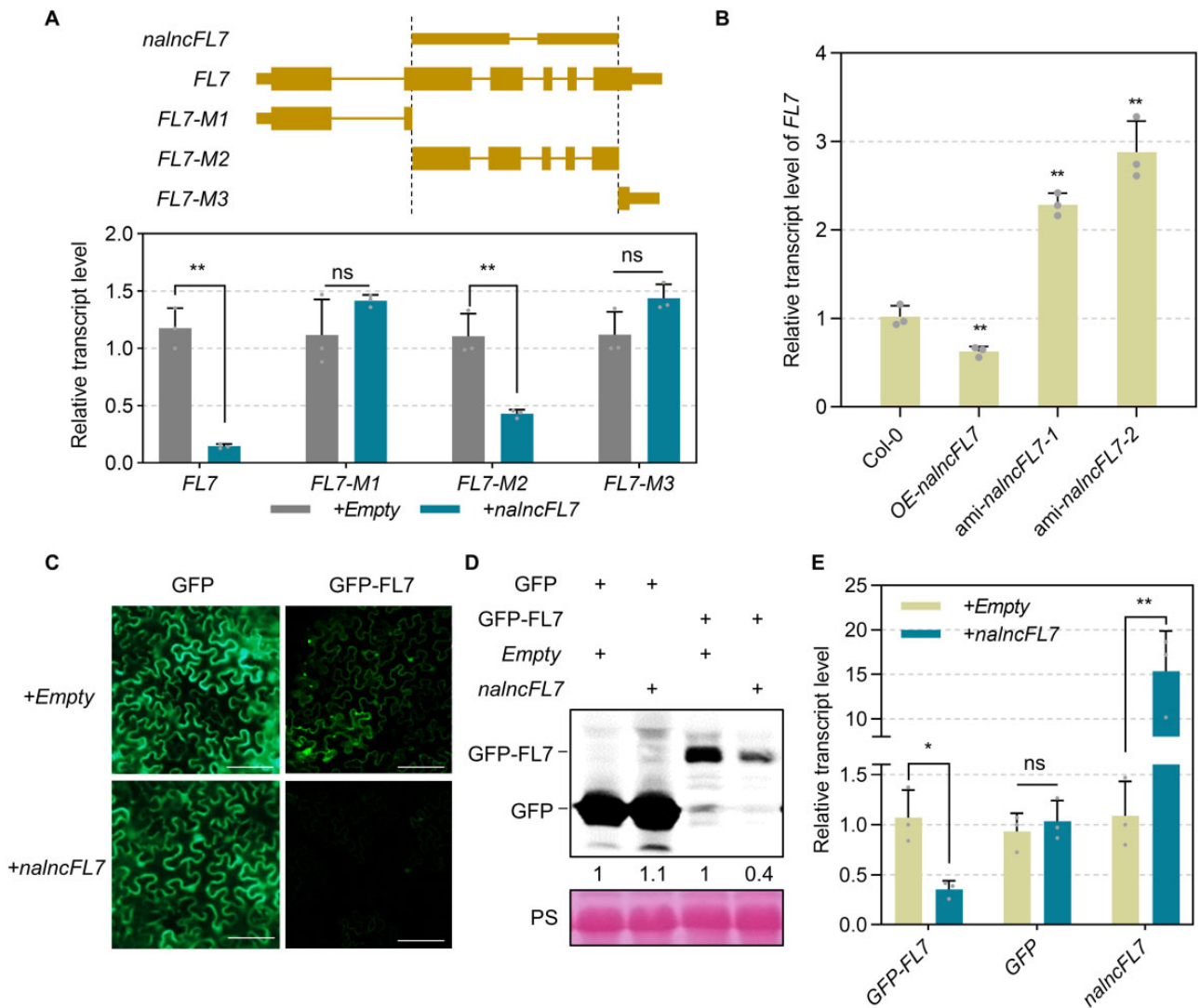


Figure 4 *nalncFL7* suppresses *FL7* accumulation. **A**, *nalncFL7* inhibition of *FL7* accumulation in Arabidopsis protoplasts. *FL7* or *FL7-M1/2/3* was co-expressed with *nalncFL7* or an empty vector in Arabidopsis protoplasts. Relative RNA levels of *FL7* and *FL7-M1/2/3* were detected by RT-qPCR. Data are means \pm SD of three biological replicates ($n = 3$; ** $P < 0.01$, Student's t test). **B**, Relative transcript levels of *FL7* in *OE-nalncFL7*, *ami-nalncFL7-1*, and *ami-nalncFL7-2* lines. The *UBQ10* gene was used as an endogenous control. Data are means \pm SD of three biological replicates ($n = 3$; ** $P < 0.01$, Student's t test, ns = not significant). **C–E**, *nalncFL7* leads to lower *FL7* abundance in *N. benthamiana*. *GFP-FL7* was co-expressed with empty or *nalncFL7* in *N. benthamiana* leaves. *GFP* was used as control. Confocal images are shown in **(C)**. Scale bars, 50 μ m. Protein levels derived from the indicated constructs are shown in **(D)** above the Ponceau S (PS)-stained membrane, which serves as loading control. Relative transcript levels of *GFP-FL7*, *GFP*, and *nalncFL7* are shown in **(E)**, as measured by RT-qPCR. *UBQ10* was used as an endogenous control. Data are means \pm SD of three biological replicates ($n = 3$; * $P < 0.05$, ** $P < 0.01$, Student's t test, ns = not significant). Numbers below the blots represent the blot band intensity of *GFP-FL7* or *GFP* with *nalncFL7* relative to those with empty vector.

phosphatase activity in the presence of *FL7* (Figure 6A). A kinetic assay of HAI1 phosphatase activity indicated that the K_m of HAI1 with or without *FL7* is 89.6 μ M (95% confidence interval [CI]: 43.18–126.3) or 72.33 μ M (95% CI: 60.63–136.7), respectively. The corresponding V_{max} values were 306.3 nmol/min (95% CI: 249.4–396.4 nmol/min) and 253.4 nmol/min (95% CI: 213.9–311.6 nmol/min), respectively (Figure 6B). These results suggested that the phosphatase activity of HAI1 is inhibited by *FL7* in vitro. We further examined whether *FL7* can inhibit other HAI proteins and

determined that *FL7* also weakly inhibits the activity of HAI2 (Figure 6C).

We then compared PP2C activity among the wild type, *fl7*, *fl7 gFL7*, and *fl7 OE-FL7* lines in vivo. In this experiment, we used okadaic acid, which inhibits the activity of other PP family phosphatases but not PP2C family proteins (Zhao et al., 2017), to accurately measure enzymatic activity of PP2C including HAI. The *fl7 OE-FL7* line exhibited significantly lower PP2C activity than the wild type or *fl7 gFL7*, whereas *fl7* showed the highest activity (Figure 6D). These

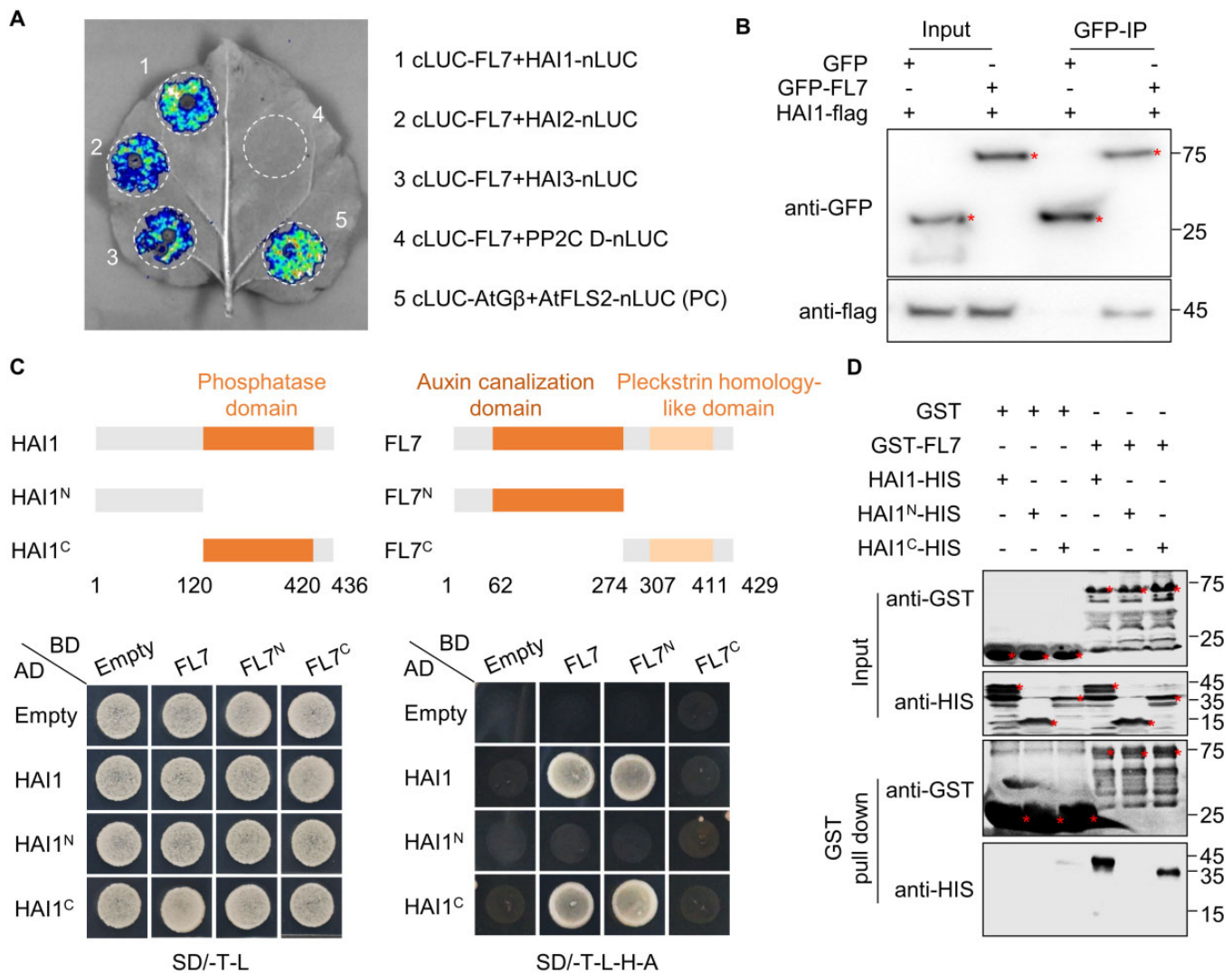


Figure 5 FL7 interacts with PP2C protein HAI1. A, Interaction tests of FL7 with HAI proteins. Luciferase complementation assays were performed in *N. benthamiana* leaves via *Agrobacterium*-mediated transient expression of the indicated constructs. The combination of *cLUC-AtGβ* and *AtFLS2-nLUC* was used as a positive control. *cLUC-FL7* and *PP2C D-nLUC* (*At5g02760*) were used as a negative control. B, Verification of the interaction between FL7 and HAI1 by Co-IP assay. Total proteins were extracted from *Arabidopsis* protoplasts expressing the indicated proteins. Interacting protein complexes were immunoprecipitated with anti-GFP beads and the bound proteins were detected by immunoblotting with anti-flag antibodies. C, Verification of the interaction between FL7 and HAI1 by Y2H. Schematic diagram of HAI1, FL7 proteins, and related truncations is shown in the upper panel. Y2H results are shown in the lower panel. D, Verification of the interaction between FL7 and HAI1 by pull-down assay. Interacting protein complexes were immunoprecipitated with anti-GST beads, and the bound proteins were detected by immunoblotting. All experiments were performed three times with similar results.

results further support the idea that FL7 is an inhibitor of HAI family phosphatases.

FL7 promotes MPK3/6 activity by inhibiting HAI1 phosphatase activity

As HAI1 was reported to dephosphorylate activated MPK3/6 (Mine et al., 2017), we incubated recombinant HAI1 with phosphorylated MPK3/6, and found that HAI1 indeed attenuates the phosphorylation of both MPK3 and MPK6 in vitro (Figure 6E and Supplemental Figure S11A). Furthermore, we added recombinant purified FL7 in this system, which restored HAI1-mediated attenuation of MPK3/6 phosphorylation in a dose dependent manner (Figure 6F

and Supplemental Figure S11B). As a control, FL7 did not affect the phosphorylation level of MPK3/6 in the absence of HAI1 (Supplemental Figure S11, C and D).

We then tested MAPK phosphorylation levels in wild type, *fl7*, *fl7 gFL7*, and *fl7 OE-FL7* after treatment with the well-known pathogen-associated molecular patterns (PAMPs) *nlp20* and *flg22* (Sun et al., 2013; Albert et al., 2019). We observed that MAPK phosphorylation decreases in the *fl7* mutant but increases in *fl7 OE-FL7* (Figure 6, G and H), indicating that FL7 positively regulates MAPK phosphorylation in vivo. At the same time, *HAI1* transcript levels showed no significant difference in Col-0, *bpl3*, or *fl7* mutant plants (Supplemental Figure S11E), suggesting that FL7

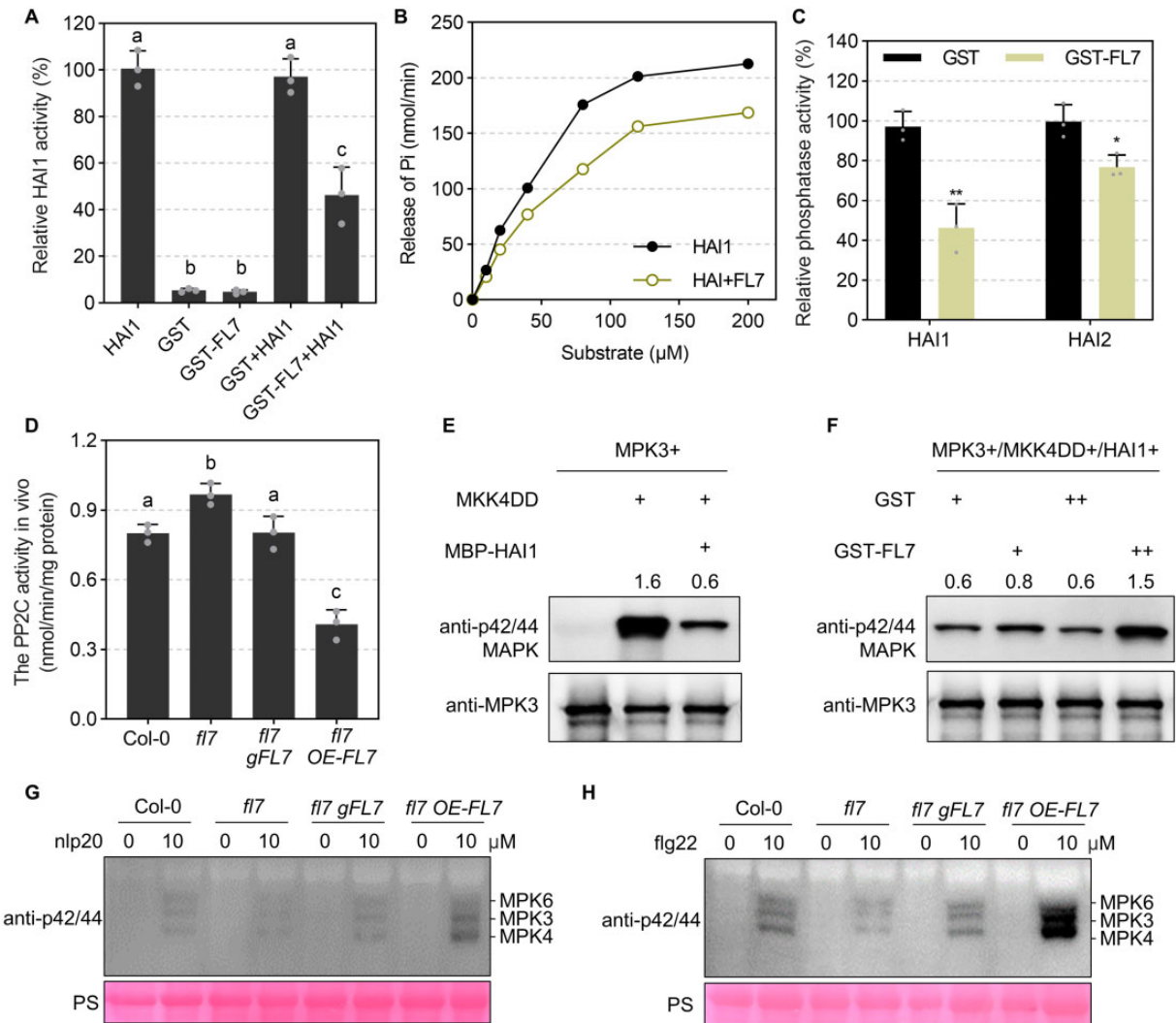


Figure 6 FL7 promotes MPK3/6 activity by inhibiting the phosphatase activity of HAI1. **A**, FL7 inhibits the phosphatase activity of HAI1 in vitro. Recombinant HAI1 (2 μg) and FL7 (4 μg) proteins were used for phosphatase activity assays. GST (4 μg) was used as a control. Substrate concentration was 100 μM. The phosphatase activity of HAI1 alone was set to 100%. Data are means ± SD of three technical replicates (lowercase letters indicate significant differences between multiple groups by one-way ANOVA at $P < 0.05$). Experiments were performed three times with similar results. **B**, Kinetics of HAI1 phosphatase activity with or without FL7. Recombinant proteins of HAI1 (2 μM) and FL7 (4 μM) were used for phosphatase activity assays. The substrate concentrations were 10, 20, 40, 80, 120, and 200 μM, and HAI1 phosphatase activity was measured using each concentration of substrate. The calculated K_m of HAI1 with or without FL7 was 89.6 μM (95% CI: 43.18–126.3 μM) or 72.33 μM (95% CI: 60.63–136.7 μM), respectively, and the V_{max} was 306.3 nmol/min (95% CI: 249.4–396.4 nmol/min) and 253.4 nmol/min (95% CI: 213.9–311.6 nmol/min), respectively. The experiments were performed three times with similar results, and the Michaelis parameters were calculated based on all three measurements. **C**, Phosphatase activity of HAI1/2. Recombinant HAI1 (2 μg) or HAI2 (2 μg) was mixed with GST (4 μg) or GST-FL7 (4 μg) for phosphatase activity assays. The phosphatase activity of HAI1 or HAI2 without FL7 was set to 100%. Substrate concentration was 100 μM. Data are means ± SD of three technical replicates ($n = 3$; * $P < 0.05$, ** $P < 0.01$, Student's t test, ns = not significant). The experiments were performed three times with similar results. **D**, Total PP2C activity in the indicated lines. Total proteins were extracted from 10-day-old seedlings. PP2C activity was measured after the addition of 5 μM okadaic acid to inhibit the activity of PP1 and PP2A family Ser/Thr-specific phosphoprotein phosphatases. Data are means ± SD of three biological replicates ($n = 3$; lowercase letters indicate significant differences tested between multiple groups by one-way ANOVA at $P < 0.05$). PP2C activity is represented as the amount of phosphate dephosphorylated by PP2C released per minute. **E**, HAI1 dephosphorylates MPK3 in vitro. Recombinant MAPKs were phosphorylated by GST-MKK4DD. Phosphorylated MAPKs (500 ng) were then mixed with MBP (2 μg) or MBP-HAI1 (2 μg) and incubated at 30°C for 15 min. Proteins were detected by immunoblotting using the indicated antibodies. Experiments were performed three times with similar results. **F**, FL7 inhibits HAI1-mediated dephosphorylation of MPK3 in vitro. Recombinant MAPKs were phosphorylated by GST-MKK4DD. Phosphorylated MAPKs (500 ng) and MBP-HAI1 (2 μg) were mixed with GST (2 or 4 μg) or GST-FL7 (2 or 4 μg) and incubated at 30°C for 15 min. Proteins were detected by immunoblotting using the indicated antibodies. Numbers above the blots (**E** and **F**) represent the blot band intensity of MPK6 blotted with anti-p42/44 antibody relative to that of MPK6 blotted with the anti-MPK6 antibody. Experiments were performed three times with similar results. **G** and **H**, MAPK activation after nlp20 (**G**) or flg22 (**H**) treatment. Phosphorylated MAPKs were detected by immunoblotting with an anti-p42/44 antibody. The expected identities of the respective bands are marked on the right. This experiment was performed three times with similar results.

regulates PAMP-triggered MPK3/6 phosphorylation by inhibiting HAI1 activity but not *HAI1* transcription. Furthermore, we tested *P. capsici* resistance in *hai1-2* (SALK_108282), and found that *P. capsici* resistance is significantly enhanced in the mutant (Supplemental Figure S11F). In addition, nlp20-induced MPK3/6 phosphorylation was also strengthened in *hai1-2* (Supplemental Figure S11G).

HAI1-mediated susceptibility did not diminish effector triggered immunity (ETI) (Mine et al., 2017). We thus wondered whether the effect of HAI1 might be similar to the susceptibility of the *fl7* mutant. As a control, we showed that flg22/nlp20-triggered ROS bursts are impaired in the *fl7* mutant (Supplemental Figure S12, A and B). Compared with Col-0, the *fl7* mutant was more susceptible to both *Pst* DC3000 (wild type) and *Pst* DC3000 (*hrcC*⁻), a strain lacking a functional type-III secretion system (T3SS) (Supplemental Figure S12, C and D). By contrast, we observed no significant difference in resistance between Col-0 and the *fl7* mutant when infected with *Pst* DC3000 carrying avirulent genes (*AvrRpt2* or *AvrRpm1*) (Supplemental Figure S12, E and F). These results indicate that FL7 regulates pattern triggered immunity (PTI) by modulating the phosphatase activity of HAI1 and subsequently the activity of MAP kinases.

As FL7 is involved in PTI, we further analyzed the transcript patterns of *FL7*, *nalncFL7*, and *BPL3* upon nlp20 treatment. *FL7* expression was first induced and then declined, peaking at 9 h (Supplemental Figure S12G). By contrast, levels of *nalncFL7* first declined and then recovered after nlp20 treatment, with a trough at 6 h (Supplemental Figure S12G). Importantly, the transcript levels of *BPL3* first declined and then recovered after nlp20 treatment, following a pattern similar to that of *nalncFL7* (Supplemental Figure S12G), supporting the notion that *BPL3*, *nalncFL7*, and *FL7* form a signaling cascade in plant immunity response.

BPL3 and FL7 are conserved across different plants

We wondered whether the *BPL3*–*nalncFL7*–*FL7* cascade might be conserved across different species. We previously showed *BPL3* was conserved across land plants (Li et al., 2019). To determine if *FL7* was similarly conserved in plants, we searched for homologs in other plant species by BLAST analyses. *FL7* homologs were ubiquitous in all the tested plants, including rapeseed (*Brassica napus*), cassava (*Manihot esculenta*), soybean (*Glycine max*), potato (*Solanum tuberosum*), and rice (Figure 7A). All homologs contained an N-terminal auxin canalization domain and a C-terminal Pleckstrin-like domain (Supplemental Data Set S3), which indicated that *FL7*, as well as *BPL3*, are conserved in plants. We also identified *nalncFL7* in these species by analyzing available strand-specific RNA-seq datasets. We identified *nalncFL7* homologs in *B. napus*, but not in other plant species (Figure 7, A and B).

Discussion

The rising number of crop diseases caused by plant pathogens, together with environmental considerations, motivates

the development of effective genetic strategies for disease management. Removal or inactivation of negative regulators of immunity in the host can potentially reduce infection and generate broad-spectrum resistance (Pavan et al., 2010; Li et al., 2021). For instance, knocking out all six *TaMLO* (*Mildew resistance locus o*) homoeologs in wheat (*Triticum aestivum*) produced plants with increased resistance to powdery mildew (Wang et al., 2014). Thus, it is important to identify such genes and study their underlying mechanisms. We previously reported that BPL family proteins are conserved negative regulators of plant immunity, among which *BPL3* makes a major non-redundant contribution to this function (Li et al., 2019). Here, we confirmed that *BPL3* was a negative regulator of immunity by complementing the *bpl3* mutant. By analyzing RNA-seq data, we discovered that *FL7* and its natural antisense lncRNA, *nalncFL7*, were regulated by *BPL3*, with *FL7* elevated and *nalncFL7* decreased in the *bpl3* mutant. *FL7* positively regulates plant immunity while *nalncFL7* is a negative regulator of resistance. We determined that *BPL3* directly bound to *nalncFL7* through its RRM domain and enhanced the stability of *nalncFL7* transcripts. Accumulated *nalncFL7* further suppressed *FL7* transcripts accumulation. Furthermore, *FL7* inhibited the phosphatase activity of HAI1, thus promoting the phosphorylation levels of MPK3/6, and eventually enhancing immunity responses. Collectively, we report the *BPL3*–*nalncFL7*–*FL7* cascade that coordinates plant immunity (Figure 7C).

The role of RRM proteins in plant–pathogen interactions and their underlying mechanisms are still largely unknown. An RRM protein in rice, PIBP1, was reported as a positive regulator of rice immunity (Zhai et al., 2019). However, this function is not related to its RNA-binding activity, although PIBP1 can associate with RNA. Rather, PIBP1 acts as a transcription factor to activate the expression of defense-related genes by binding to DNA (Zhai et al., 2019). In this study, we identified the cis-natural antisense lncRNA, *nalncFL7*, to which *BPL3* bound. We demonstrated that *BPL3* negatively regulated plant immunity by binding and stabilizing *nalncFL7* transcripts. Such findings will improve our knowledge when exploring the mechanisms underlying the function of other RRM proteins.

The expression of nalncRNAs is often positively or negatively correlated with their cognate sense genes with distinct underlying mechanisms (Kindgren et al., 2018; Zhao et al., 2018; Wu et al., 2020). For example, *MAS*, a nalncRNA produced from *MADS AFFECTING FLOWERING4* (*MAF4*), recruits WDR5a and then guides COMPASS-like complexes to the *MAF4* promoter to enhance *MAF4* transcription (Zhao et al., 2018). In another example, the cold-induced antisense transcript *SVALKA-asCBF1* suppresses C-REPEAT/DRE BINDING FACTOR1 (*CBF1*) by RNA polymerase II collision (Kindgren et al., 2018). Alternatively, some nalncRNAs may downregulate sense transcripts by forming double-stranded RNA with sense transcripts and producing siRNAs (Katiyar-Agarwal et al., 2006; Li et al., 2020). In this study, we determined that *nalncFL7* overexpression lowered the levels of its

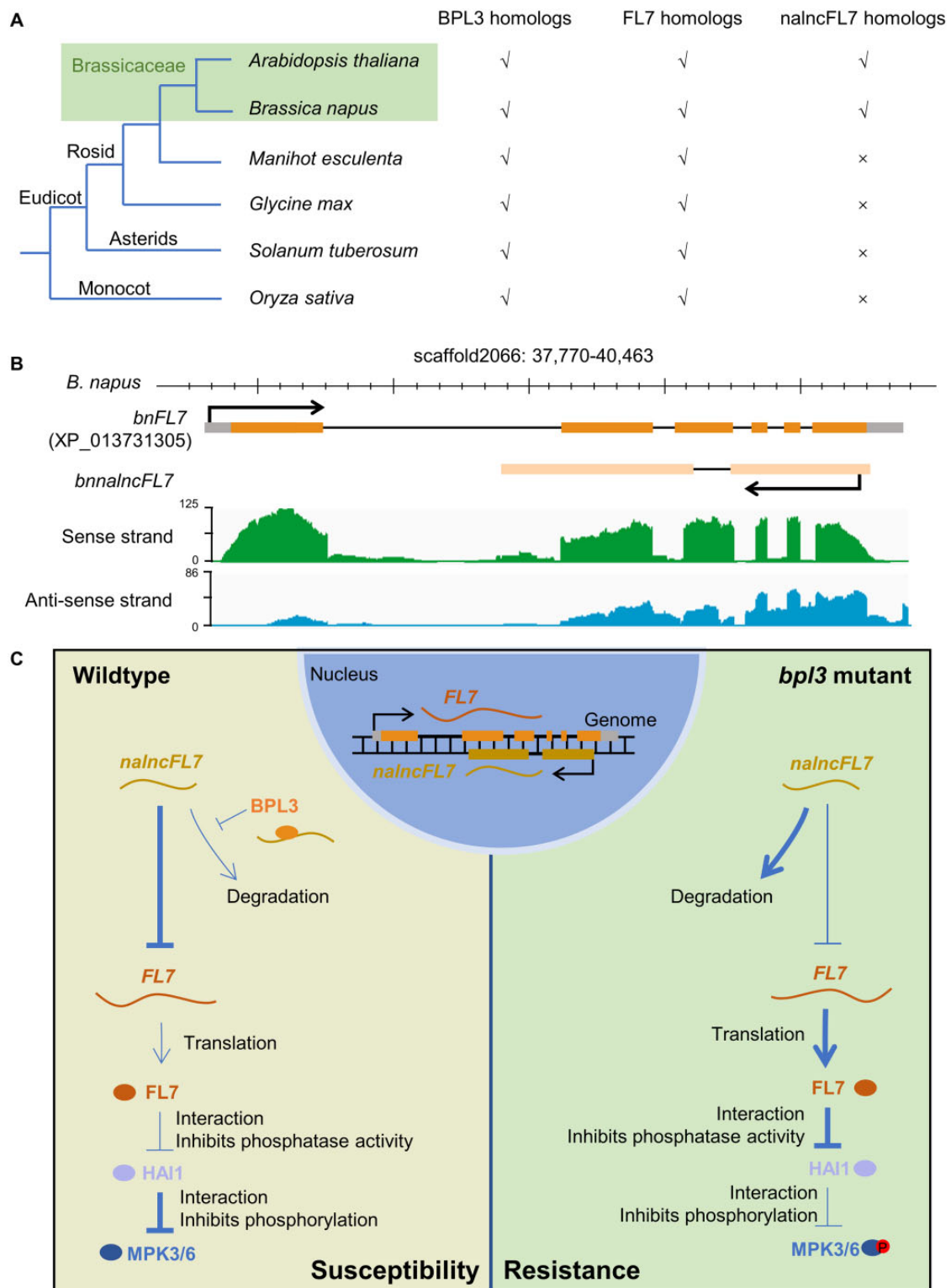


Figure 7 BPL3–*nalncFL7*–FL7 cascade is conserved in Brassicaceae. **A**, BPL3, FL7, and *nalncFL7* in different species. Tick marks means that the species contains the indicated homologs, while crosses mean the species do not. The phylogenetic tree of species was obtained from Phytozome. **B**, Transcript abundance of *FL7* and *nalncFL7* in *B. napus*. RNA-seq data of *B. napus* was mapped to its reference genome. IGV browser views of RNA-seq signals at *FL7* and *nalncFL7* with normalized read counts per million along the y-axis are shown. **C**, Schematic diagram illustrating how the BPL3–*nalncFL7*–FL7 cascade regulates plant immunity. Solid terminated lines represent inhibition. One-way solid arrows represent promotion. In normal conditions, BPL3 binds to *nalncFL7* and stabilizes *nalncFL7* transcripts. When plants are exposed to pathogens, the transcript levels of BPL3 decrease, leading to *nalncFL7* transcript degradation and thus the release of its suppression on *FL7*. *FL7* inhibits the phosphatase activity of HAI1, enhancing MPK3/6 activity and finally activating plant immunity. In the *bpl3* mutant, *FL7* transcripts consistently accumulate, making the *bpl3* mutant more resistant compared with the wild type.

sense transcript *FL7*, while knockdown of *nalncFL7* led to *FL7* transcript accumulation, indicating that *nalncFL7* also negatively regulates its cognate sense transcript. It is still unknown how *nalncFL7* suppresses *FL7*. Since the complementary region of *nalncFL7* and *FL7* is vital for this suppression (Figure 4A), we speculate that *nalncFL7* may directly bind to *FL7* transcripts to form double-stranded RNA and suppress *FL7* accumulation in a small RNA-dependent manner.

An interesting finding is that *FL7* is an inhibitor of HAI1, a PP2C A protein. Type A PP2Cs do not contain regulatory subunits but have conserved C-terminal catalytic domains that interact with and are inhibited by ABA-bound PYR1/PYL/RCARs (Fujii et al., 2009; Park et al., 2009; Hao et al., 2011). However, it is currently unknown whether this catalytic domain is regulated by other proteins. Our genetic and biochemical analyses indicated that *FL7* directly bound to the catalytic domain of HAI1, inhibiting its PP2C activity and thus promoting MAPK phosphorylation. Similar to PYR1/PYL/RCARs, *FL7* interacted with the same catalytic domain of HAI1, raising the possibility that *FL7* may inhibit HAI1 activity in the same manner as PYR1/PYL/RCARs. Compared with protein serine/threonine kinases (PSKs), there are fewer PSPs: the human genome encodes 428 PSKs versus 31 PSPs, whereas in Arabidopsis, there are 1,000 PSKs but only 102 PSPs (Kerk et al., 2008; Shi, 2009). The way these PSPs are dynamically regulated by different proteins or compounds has garnered increasing attention over the past few years. We envisage that our findings are the tip of a PSPs regulatory network iceberg.

Substantial evidence has shown that a tight crosstalk exists between ABA regulatory pathways and plant defense responses. For example, the HAI proteins respond to the defense signal jasmonate–isoleucine (Mine et al., 2017). The ABA receptor PYR1 that regulates the immune response (Garcia-Andrade et al., 2020) interacts with and regulates the HAI proteins and the PP2C ABA INSENSITIVE 1 (Tischer et al., 2017). Our results revealed that *FL7* might emerge as another key transducer shared between ABA and immune responses. The abundance of *FL7* transcripts responded to pathogen signals and *FL7* can inhibit the activity of HAI1, a key regulator of ABA response pathway. It remains an open question whether *FL7* functions in the ABA response pathway and how *FL7* integrates defense response and ABA signaling to facilitate plant adaptation to complex environments.

We discovered that *BPL3* and *FL7* were conserved in land plants, while *nalncFL7* was only conserved in the Brassicaceae, which indicates that the *BPL3–nalncFL7–FL7* cascade might have arisen after the emergence of Brassicaceae species. It is still unknown whether *BPL3* can regulate *FL7* outside the Brassicaceae. However, as all *FL7* homologs contained an N-terminal auxin canalization domain and a C-terminal Pleckstrin-like domain, it is possible that *FL7* homologs are conserved HAI1 regulators in land plants.

FL7 is upregulated and *nalncFL7* is downregulated upon PAMP treatment, indicating that *FL7* accumulates when hosts are exposed to pathogens to inhibit HAI1 activity and enhance MAPK-mediated immunity. Notably, *nalncFL7* transcripts increase again coupled with declining transcripts level of *FL7* at a late stage into treatment with PAMPs. Thus, the existence of *nalncFL7* may provide fitness advantages, possibly by suppressing *FL7* transcript accumulation in the absence of pathogens to control the intensity and timing of MPK3/MPK6 activation in Arabidopsis and possibly in other species. Additionally, *BPL3* and *nalncFL7* shared nearly the same transcript accumulation pattern, which was antagonistic to that of *FL7* (Supplemental Figure S9A), indicating that the *BPL3–nalncFL7–FL7* cascade also exists in different tissues. These findings provide a framework for explaining the mechanism by which hosts regulate MAPK cascades under pathogen attack in different tissues.

In Arabidopsis, *BPL3*, *FL7*, or HAI1 is one member of a protein family that contains several homologs (Zhang et al., 2020). Thus, the *BPL3–nalncFL7–FL7–HAI1* cascade is likely one facet of a more complex network. Our data suggest additional regulatory interactions between *BPL3* and other *FKD1/FL* family members (Supplemental Figure S7). Furthermore, *FL7* interacted with HAI2/3 and inhibited HAI2 activity (Figures 5A and 6C), indicating that *FL7* might interact with and inhibit multiple PP2C A proteins. In addition, the BioGRID database indicated that *FL7* interacted with as many as nine ABA pathway target proteins in addition to HAI1 and ABI1, including the ABA-responsive transcription factor ABI5 (Supplemental Figure S10). A complex network centered on *BPL3* and *FL7* may thus encompass all these components, potentially integrating a plethora of physiological and developmental processes and environmental responses. It will be worthwhile to unravel this network in the future.

In conclusion, we propose the following working model, by which the *BPL3–nalncFL7–FL7* cascade coordinates plant immunity. In normal conditions, the cascade fine-tunes HAI1-mediated dephosphorylation of MPK3/6 to maintain proper immunity levels. When plants are exposed to pathogens, MPK3/6 activation will be boosted by this cascade because downregulated *BPL3* will lead to *FL7* accumulation to release the inhibition of MPK3/6 by HAI1, and eventually evoke plant immunity. The *bp13* mutant consistently accumulates *FL7* transcripts and is more resistant compared with the wild type. Understanding the underlying mechanisms may open the possibility to explore how plant immunity is precisely adjusted to counteract pathogen invasion with minimum negative effects.

Materials and methods

Plant materials and growth conditions

Arabidopsis (*A. thaliana*) and *N. benthamiana* plants were grown and maintained in plant growth chambers at an ambient temperature of 23°C under a 16-h light/8-h dark photoperiod. Light was provided by white fluorescent bulbs

with an intensity of $\sim 120 \mu\text{mol m}^{-2} \text{s}^{-1}$. All Arabidopsis lines used in this study were in a Col-0 accession. T-DNA insertion mutants (*fl7*, SALK_077717C; *hai1-2*, SALK_108282C) were obtained from Arashare (<https://www.arashare.cn/index/>). The *fl7 bpl3* double mutant was generated by crossing *fl7* and *bpl3* single mutants. Homozygous T-DNA insertion plants were verified by genomic PCR with T-DNA primer LB1.3 and gene-specific primers, which were designed as described by the Salk Institute Genomic Analysis Laboratory website (<http://signal.salk.edu/>).

To generate complementation transgenic lines expressing FLAG-tagged *BPL3* or *FL7*, a DNA fragment encoding *BPL3* or *FL7* was fused to a C-terminal $3 \times$ FLAG tag and cloned into the pSuper vector. To generate transgenic lines overexpressing FLAG-tagged *FL7*, the sequence encoding *FL7* was fused to a C-terminal $3 \times$ FLAG tag and cloned into the pSuper vector. *amiRNAs* constructs targeting *nalncFL7* were constructed using pre-miR319a as backbone, as described (Schwab et al., 2006). All constructs were introduced into *Agrobacterium* (*Agrobacterium tumefaciens*) strain GV3101 for plant transformation using the floral dip method (Clough and Bent, 1998). Positive transformants were recovered by antibiotic selection and confirmed by genomic PCR, RT-qPCR, and/or immunoblot analysis.

P. capsici culture conditions and inoculation assays

The *P. capsici* strain LT263 used in this study was cultured and maintained at 25°C in the dark on 10% (v/v) V8 juice medium. The zoospore inoculation of Arabidopsis was performed as described previously (Li et al., 2019). Briefly, *P. capsici* mycelium was grown in liquid V8 medium for 3 days, washed three times with sterilized water, and then incubated in sterilized water at 25°C in darkness until the formation of sporangia. The cultures were placed at 4°C for 20 min to initiate zoospore release. Approximately 500 *P. capsici* zoospores were dropped at the center of each detached leaf for inoculation. Inoculated leaves were photographed under UV light and lesion areas were measured at the indicated time points.

Measurement of RNA stability

To inhibit transcription, 200 $\mu\text{g/mL}$ actinomycin D (Act D) (Sigma Aldrich, Saint Louis, Missouri, USA) in 0.1% dimethyl sulfoxide (DMSO) was infiltrated into the indicated leaves. An equivalent volume of 0.1% DMSO alone was used as a control. The leaves were collected at the indicated times for RT-qPCR. Transcript levels were normalized to those of the control gene *GAPDH* (for *FL7*, *nalncFL7*, and *UBQ10*) or *UBQ10* (for *GAPDH*), and to RNA from DMSO-treated control samples for each experiment.

Protein purification

Proteins with different tags were expressed in Rosetta (DE3) *Escherichia coli* cells growing in LB medium with 0.5 mM IPTG for 18 h at 18°C. The culture was then collected by centrifugation at 6,000 g for 10 min at 4°C. For His-tagged proteins, the pellet was resuspended in lysis buffer (50 mM

NaH_2PO_4 , 30 mM NaCl, 10 mM imidazole, pH 8.0, 1 mM PMSF, and protease inhibitor cocktail [Abmart, A10004]) then sonicated for 10 min. After centrifugation for 30 min at 7,000 g and 4°C, the supernatant was incubated with Ni Sepharose (GE) resin for 3 h at 4°C. The resin was washed three times with washing buffer (50 mM NaH_2PO_4 , 30 mM NaCl, and 50 mM imidazole, pH 8.0) to remove non-specifically bound proteins. The His-tagged proteins were eluted from the resin with elution buffer (50 mM NaH_2PO_4 , 30 mM NaCl, and 250 mM imidazole, pH 7.4). For GST-tagged proteins, the pellet was resuspended in phosphate-buffered saline (PBS) (150 mM NaCl, 10 mM Na_2HPO_4 , 2 mM KH_2PO_4 , 2.7 mM KCl, pH 7.4, 1 mM PMSF, and inhibitor cocktail) then sonicated for 10 min. After centrifugation for 30 min at 7,000 g and 4°C, the supernatant was incubated with glutathione Sepharose 4B (GE) resin for 3 h at 4°C. The resin was washed three times with PBS to remove non-specifically bound proteins. The GST-tagged proteins were eluted from the resin with GSH buffer (50 mM Tris-HCl, pH 8.0, and 10 mM GSH). For MBP-tagged proteins, the pellet was resuspended in lysis buffer (20 mM Tris-HCl, pH 7.4, 200 mM NaCl, 1 mM EDTA, 1 mM PMSF, and inhibitor cocktail) then sonicated for 10 min. After centrifugation for 30 min at 7,000 g and 4°C, the supernatant was incubated with amylose resin (NEB) for 3 h at 4°C. The resin was washed three times with lysis buffer to remove non-specifically bound proteins. The MBP-tagged proteins were eluted from the resin with elution buffer (20 mM Tris-HCl, pH 7.4, 200 mM NaCl, 1 mM EDTA, and 10 mM maltose). To measure their concentrations, the purified proteins were mixed with Quick Start Bradford Dye Reagent (Bio-Rad), and the absorbance was measured at 595 nm. Protein concentrations were calculated based on a standard curve with bovine serum albumin (BSA) as a substrate.

Protein pull-down assay

The coding sequences of the genes of interest were cloned into the pET-28a vector or the pGEX-6P vector. Recombinant HAI1-6XHIS, GST, and GST-FL7 proteins were purified as described above. Purified GST or GST-FL7 (10 mg) in 2 mL lysis buffer (150 mM NaCl, 10 mM Na_2HPO_4 , 2 mM KH_2PO_4 , 2.7 mM KCl, pH 7.4, 1 mM PMSF, and inhibitor cocktail) was incubated with glutathione beads for 2 h at 4°C. After a brief centrifugation at 1,000 g for 3 min at 4°C, the buffer was removed and 2 mg of recombinant HAI1-6XHIS protein was added to the resin in 2 mL of lysis buffer. The tube was rotated at 4°C for 2 h for protein binding. The resin was then washed five times with PBS to remove non-specifically bound protein, then resuspended in 50 μL of PBS and 10 μL of SDS loading buffer, and boiled for 5 min. After centrifugation at 12,000 g for 1 min at 22°C, the supernatant was subjected to immunoblotting analysis. Immunoblot assays were conducted with anti-GST (1:5,000; #M20007; Abmart) or anti-HIS (1:5,000; #M20001; Abmart) antibodies and HRP-conjugated anti-mouse IgG (1:10,000, Sigma-Aldrich) as secondary antibody.

RNA-pull down assay

Biotin-labeled RNAs were obtained by using Biotin RNA Labeling Mix (Roche) and T7 RNA polymerase (Roche). Recombinant proteins were purified using a bacterial expression system as above. Two micrograms of biotin-labeled RNAs and recombinant proteins were mixed in pull-down buffer (50 mM Tris-HCl, pH 7.5, 150 mM NaCl, 2 mM dithiothreitol [DTT], 0.05% [v/v] Nonidet P-40, and protease inhibitor [Roche]) and incubated for 6 h at 4°C. Thirty microliters of washed streptavidin agarose beads (Sigma) was then added to each binding reaction and further incubated for 2 h at 4°C. Beads were washed briefly five times using binding buffer and boiled in SDS buffer, and the supernatant was analyzed by immunoblotting.

Measurement of PP2C activity

PP2C activity was measured using a Ser/Thr Phosphatase Assay Kit (Promega, V2460). In brief, the recombinant proteins were purified with buffers that did not contain phosphate. To measure phosphatase activity, different combinations of recombinant purified FL7 and HAI1 were mixed with 5 µL of 1 mM phosphopeptide and 10 µL of PP2C reaction buffer (250 mM imidazole, pH 7.2, 1 mM EGTA, 25 mM MgCl₂, 0.1% [v/v] β-mercaptoethanol, and 0.5 mg/mL BSA) in the wells of a microtiter dish, then incubated at 25°C for 15 min. The reactions were stopped by adding 50 µL of molybdate dye/additive mixture, then the plate was incubated at room temperature for 15 min. The absorbance was measured at 630 nm in a Microplate Reader (Molecular Devices, SpectraMax M5). Michaelis–Menten plots in GraphPad Prism 9.0 were used to calculate the kinetic parameters.

To measure PP2C activity in vivo, total proteins (0.1 g) from the wild type, *fl7*, *fl7 gFL7*, or *fl7 OE-FL7* were extracted using phosphatase storage buffer (20 mM Tris-HCl, pH 7.5, 20 mM KCl, 1 mM EDTA, 1 mM EGTA, 10 mM DTT, 0.5% [v/v] Triton X-100, and 50% [v/v] glycerol) with protease inhibitor cocktail (Abmart, A10004), then the homogenized lysate was centrifuged at 100,000 g for 1 h at 4°C. The supernatant was filtered through Sephadex G-25 resin to remove endogenous phosphates, then the lysate was used to measure PP2C activity as described above but with the addition of 5 µM okadaic acid.

MAP kinase assays

MAP kinase assays were performed essentially as described previously (Zhang et al., 2018b). For MAMP-triggered MAPK activation, 30-day-old Arabidopsis plants were used. Appropriate chemicals were infiltrated into leaves. The leaves were then frozen in liquid nitrogen and stored at -80°C. The frozen leaves were ground in liquid nitrogen and homogenized in MAPK extraction buffer (50 mM Tris-HCl, pH 7.5, 5 mM EDTA, 5 mM EGTA, 2 mM DTT, 10 mM sodium fluoride, 50 mM β-glycerolphosphate, 10% [v/v] glycerol, complete proteinase inhibitor cocktail [Roche, Mannheim, Germany], and Phosstop phosphatase inhibitor cocktail [Roche]). The proteins were separated on a 10%

polyacrylamide gel. Immunoblot analysis was performed using anti-phospho-p44/42 MAPK (1:5,000, Cell Signaling Technology, Danvers, Massachusetts, USA; #9101), anti-AtMPK3 (1:2,500, Sigma; M8318), anti-AtMPK6 (1:5,000, Sigma; M7104) as first antibodies, and HRP-conjugated anti-rabbit IgG (1:10,000, Sigma-Aldrich; A6154) or HRP-conjugated anti-mouse IgG (1:10,000, Sigma-Aldrich), as secondary antibodies.

In vitro dephosphorylation of MAPK

Escherichia coli strain Rosetta (DE3) was used for production of recombinant proteins. To prepare phosphorylated MPK3 and MPK6, 5 µg of recombinant purified MBP-tagged kinase-inactive MAPK was incubated with 1 µg of GST-MKK4DD at 30°C for 1 h in kinase buffer (25 mM Tris-HCl, pH 7.5, 1 mM DTT, 10 mM MgCl₂, and 200 µM ATP). The kinase reaction was terminated by removing ATP from the reaction using an Amicon Ultra-30K centrifugation unit (Millipore). To test phosphatase activity of HAI1, phosphorylated MAPKs (500 ng) were incubated with MBP or MBP-HAI1 (2 µg) at 30°C for 15 min in phosphatase buffer (25 mM Tris-HCl, pH 7.5, 1 mM DTT, and 10 mM MgCl₂). MAPKs were detected by immunoblotting as described above. To test whether FL7 inhibits phosphatase activity of HAI1, phosphorylated MAPKs (500 ng) and MBP-HAI1 (2 µg) were incubated with GST or GST-FL7 at 30°C for 15 min in phosphatase buffer (25 mM Tris-HCl, pH 7.5, 1 mM DTT, and 10 mM MgCl₂).

DAB and trypan blue staining

To detect ROS bursts, inoculated leaves were stained with 1 mg/mL DAB solution for 8 h in the dark starting at 12 hpi, and then cleared with ethanol before observation by light microscopy. For trypan blue staining, a stock solution was prepared by mixing 0.02 g trypan blue, 10 g phenol, 10 mL glycerol, 10 mL lactic acid, and 10 mL distilled water. Arabidopsis leaves were soaked in the trypan blue solution overnight at room temperature. Leaves were then cleared in 95% (v/v) ethanol for 3 days with gentle shaking. Samples were then equilibrated with 70% (v/v) glycerol for photography under white light.

Transient expression in *N. benthamiana*

Agrobacterium strains containing the indicated constructs were cultured at 28°C at 220 rpm for 48 h, and then were collected by centrifugation at 23°C and 6,000 g for 2 min. The cells were washed and then resuspended in 10 mM MgCl₂ to an appropriate OD₆₀₀ of 0.4–0.6. Leaves of five-week-old *N. benthamiana* plants were infiltrated for transient expression.

Arabidopsis protoplast preparation and transfection

Protoplast preparation and transfection were performed as described previously (Li et al., 2019), except that the transfected protoplasts were incubated in W5 medium (154 mM NaCl, 125 mM CaCl₂, 5 mM KCl, and 2 mM MES, pH 5.7) instead of 0.4 M mannitol.

RT-qPCR analysis

Total RNA was extracted by using an RNA-simple Total RNA Kit (Tiangen) according to the manufacturer's instructions. *Arabidopsis* and *N. benthamiana* cDNA was synthesized with a HiScript II Q RT SuperMix for qPCR (Vazyme, <https://www.vazymebiotech.com>). Quantitative PCR was performed by using a SYBR Premix Ex Taq Kit (TaKaRa) on an ABI Prism 7500 Fast Real-Time PCR system following the manufacturer's instructions. Expression levels were normalized to the expression of *AtGAPDH* or *AtUBQ10*, which are stably expressed reference genes in *Arabidopsis*. Briefly, the threshold cycles (Ct) of tested or reference genes in different samples were calculated by a 7500 Fast Real-Time PCR system. In each sample, ΔCt was calculated by Ct (tested genes) minus Ct (reference genes) for normalization. Then $\Delta\Delta\text{Ct}$ was calculated by Ct (sample 1) minus Ct (sample 2). Finally, the amplicon amount of tested gene in sample 2 compared with that in sample 1 is defined by the equation: $2^{-\Delta\Delta\text{Ct}}$.

Immunoblot assay

To extract proteins from plant materials, leaves were frozen in liquid nitrogen and ground to a fine powder. Extraction buffer (50 mM HEPES, 150 mM KCL, 1 mM EDTA, and 0.1% [v/v] Triton X-100; pH 7.5) containing 1 mM DTT and protease inhibitor cocktail (Sigma) was used for protein extraction. Anti-GFP antibody (1:5,000; #M20004; Abmart) and HRP-conjugated anti-mouse IgG (1:10,000, Sigma-Aldrich) as secondary antibody were used for immunoblotting protein with GFP tag. mAb-HRP-Direct anti-FLAG antibody (1:5,000; #M185-7; MBL) was used for immunoblotting protein with flag tag.

Phylogenetic analysis

Multiple alignments of full-length aa sequences were aligned using MUSCLE. Phylogenetic analysis was performed using full-length sequences with the MEGA X program by the maximum-likelihood method with 100 bootstrap samples and parameters: poisson model, uniform rates, and complete deletion. Alignments data and phylogenetic tree data could be found in [Supplemental Files S1 and S2](#).

Co-IP assay

Arabidopsis protoplasts were transfected with the indicated plasmid combinations and control constructs, and transfection was performed as described above. Immunoprecipitation with anti-GFP antibodies was carried out as previously described (Ai et al., 2021). Total protein and immunoprecipitates were separated by SDS-PAGE and detected by immunoblotting.

Transcriptome sequencing and bioinformatics analysis

RNA-seq data of Col-0, *bpl3*, *bpa1*, and *bpl2* were reported previously (Li et al., 2019). The strand-specific RNA-seq data used in the study were deposited at the National Genomics Data Center database and can be downloaded from [https://](https://ngdc.cncb.ac.cn/gsa/browse/CRA007958)

ngdc.cncb.ac.cn/gsa/browse/CRA007958. For strand-specific RNA-seq in this study, total RNA was extracted from indicated plants and RNA quality was evaluated on an Agilent 2100 Bioanalyzer (Agilent Technologies, Santa Clara, California, USA). Ribosomal RNA was removed from total RNA in order to retain maximal ncRNA using a TIANSeq rRNA Depletion Kit (#NR101-T7; TIANGEN). The resulting mRNA was randomly fragmented into short fragments using an MGIEasy RNA Directional Library Prep Set (#1000006385; MGI). The fragmented mRNA was used as template to synthesize the first cDNA strand with random hexamers, after which buffer, dNTPs, RNase H, and DNA polymerase I were added for second cDNA strand synthesis. After purification with QiaQuick PCR kit (#28104; QIAGEN) and elution in EB buffer, the cDNA was end-repaired, A-tailed, and ligated to adapters. The desired fragment size was selected by gel electrophoresis, followed by PCR amplification.

All clean reads were mapped to the *Arabidopsis* reference genome (Version TAIR10) using Hisat2 with parameters: `-min-intronlen 30 -max-intronlen 5000 -dta` (Pertea et al., 2016). SAMtools was used to convert and sort SAM files (Li et al., 2009). Based on the length of each gene and the number of reads uniquely mapped to that gene, expression levels were normalized as transcripts per million reads using the Stringtie tool (Pertea et al., 2016). EdgeR was used to conduct pairwise comparisons with a cutoff (P -value ≤ 0.05 , $|\text{Fold change}| \geq 2$). The mapped reads were visualized using IGV tools (Robinson et al., 2011). Alternative splicing events were detected and quantified using rMATs (Shen et al., 2014).

GO enrichment analysis was performed using the OmicShare tools, a free online platform for data analysis (www.omicshare.com/tools). Firstly, all DEGs were mapped to GO terms in the GO database (<http://www.geneontology.org/>), the number of genes associated with each term was calculated, significantly enriched GO terms in DEGs comparing to the genome background were defined by a hypergeometric test. The calculated P -value was adjusted through false discovery rate (FDR) correction, taking $\text{FDR} \leq 0.05$ as a threshold. GO terms meeting this condition were defined as significantly enriched GO terms in DEGs. This analysis was able to recognize the main biological functions that DEGs exercise.

Statistical analysis

All data are shown as means \pm standard deviation (SD) from at least three biological repeats or from three technical replicates in one of three experiments with similar results. Two-tailed Student's t test was used for comparing means between two samples (* and ** represent $P < 0.05$ and 0.01, respectively). One- or two-way analysis of variance (ANOVA) was used for testing the significance of the difference among different group means (different lowercase letters indicate significant differences, $P < 0.05$). Detailed statistical reports are provided in [Supplemental Data Set S5](#).

Accession numbers

Sequence data from this article can be found in the TAIR (The Arabidopsis Information Resource) databases under the following accession numbers: *FL7* (At4g16670), *nalncFL7* (At4g06410), *BPL3* (At1g14340), *BPL2* (At1g67950), *BPA1* (At5g16840), *HAI1* (At5g59220), *HAI2* (At1g07430), *HAI3* (At2g29380), *FKD1* (At3g63300), *FL1* (At5g43870), *FL2* (At3g22810), *FL3* (At4g14740), *FL4* (At4g32780), *FL5* (At4g17350), *FL6* (At5g47440), *FL8* (At5g57770), *MPK3* (At3g45640), *MPK6* (At2g43790), *MKK4* (At1g51660), and *PP2C D* (At5g02760). The strand-specific RNA-seq data used in the study were deposited at the National Genomics Data Center database under the accession number CRA007958 and can be downloaded from <https://ngdc.cnbc.ac.cn/gsa/browse/CRA007958>. The RNA-seq data used in Supplemental Figure S5 were downloaded from The Sequence Read Archive of NCBI (SRR513597, SRR7727954). The RNA-seq data used in Figure 7A were downloaded from The Sequence Read Archive of NCBI (SRR7880321 and SRR7880322 for *B. napus*; SRR5221836 and SRR5221837 for *G. max*; SRR7885771 and SRR7885775 for *M. esculenta*; SRR2932329 and SRR2932330 for *S. tuberosum*; and DRR090670 and DRR090673 for *O. sativa*).

Supplemental data

The following materials are available in the online version of this article.

Supplemental Figure S1. Validation of the transgenic plants.

Supplemental Figure S2. BPL3 is a negative regulator of plant immunity.

Supplemental Figure S3. Level 2 GO enrichment analysis of genes elevated in the *bpl3* mutant compared with wild-type plants.

Supplemental Figure S4. Level 3 GO enrichment analysis of genes elevated in the *bpl3* mutant compared with wild-type plants.

Supplemental Figure S5. *FL7* and *nalncFL7* abundance in the reported RNA-seq data.

Supplemental Figure S6. Antisense transcripts of other *FL* genes.

Supplemental Figure S7. Interaction specificity of BPL3 and *FL7*.

Supplemental Figure S8. Validation of *FL7*- and *nalncFL7*-related mutants and transgenic plants.

Supplemental Figure S9. *nalncFL7* antagonizes *FL7* in transcript levels.

Supplemental Figure S10. Putative *FL7* interactors identified in BioGRID database.

Supplemental Figure S11. *FL7* inhibits HAI1-mediated dephosphorylation of MPK6.

Supplemental Figure S12. Susceptibility conferred by the *fl7* mutation does not diminish ETI.

Supplemental Data Set S1. DEGs in *bpl3* mutant compared with wild type.

Supplemental Data Set S2. Differentially spliced genes in the *bpl3* mutant compared with wild type.

Supplemental Data Set S3. *FL7* homologs identified in the indicated species.

Supplemental Data Set S4. Primers used in this work.

Supplemental Data Set S5. Summary of statistical analyses.

Supplemental File S1. Sequence alignment of *FLs* proteins.

Supplemental File S2. Phylogenetic tree of *FL* proteins in Newick format.

Acknowledgments

We appreciate Prof. Donglei Yang at Nanjing Agricultural University for valuable suggestions.

Funding

This work was supported by the National Natural Science Foundation of China (32230089, 31625023, and 32072507), the Jiangsu Funding Program for Excellent Postdoctoral Talent (2022ZB342), and the Postdoctoral innovation talent support program (BX20220153).

Conflict of interest statement. None declared.

References

- Ai G, Xia Q, Song T, Li T, Zhu H, Peng H, Liu J, Fu X, Zhang M, Jing M, et al. (2021) A *Phytophthora sojae* CRN effector mediates phosphorylation and degradation of plant aquaporin proteins to suppress host immune signaling. *PLoS Pathog* 17: e1009388
- Albert I, Zhang L, Bemm H, Nurnberger T (2019) Structure–function analysis of immune receptor AtRLP23 with its ligand nlp20 and coreceptors AtSOBIR1 and AtBAK1. *Mol Plant–Microbe Interact* 32: 1038–1046
- Borsani O, Zhu J, Verslues PE, Sunkar R, Zhu JK (2005) Endogenous siRNAs derived from a pair of natural cis-antisense transcripts regulate salt tolerance in Arabidopsis. *Cell* 123: 1279–1291
- Bouchard J, Oliver C, Harrison PM (2015) The distribution and evolution of *Arabidopsis thaliana* cis natural antisense transcripts. *BMC Genomics* 16: 444
- Breen S, Williams SJ, Outram M, Kobe B, Solomon PS (2017) Emerging insights into the functions of pathogenesis-related protein 1. *Trends Plant Sci* 22: 871–879
- Clough SJ, Bent AF (1998) Floral dip: a simplified method for Agrobacterium-mediated transformation of *Arabidopsis thaliana*. *Plant J* 16: 735–743
- Cui J, Luan Y, Jiang N, Bao H, Meng J (2017) Comparative transcriptome analysis between resistant and susceptible tomato allows the identification of lncRNA16397 conferring resistance to *Phytophthora infestans* by co-expressing glutaredoxin. *Plant J* 89: 577–589
- de Longevialle AF, Small ID, Lurin C (2010) Nuclearly encoded splicing factors implicated in RNA splicing in higher plant organ-elles. *Mol Plant* 3: 691–705
- Di C, Yuan JP, Wu Y, Li JR, Lin HX, Hu L, Zhang T, Qi YJ, Gerstein MB, Guo Y, et al. (2014) Characterization of stress-responsive lncRNAs in *Arabidopsis thaliana* by integrating expression, epigenetic and structural features. *Plant J* 80: 848–861
- Downen RH, Pelizzola M, Schmitz RJ, Lister R, Downen JM, Nery JR, Dixon JE, Ecker JR (2012) Widespread dynamic DNA methylation

- in response to biotic stress. *Proc Natl Acad Sci USA* **109**: E2183–E2191
- Duque P** (2011) A role for SR proteins in plant stress responses. *Plant Signal Behav* **6**: 49–54
- Faghihi MA, Modarresi F, Khalil AM, Wood DE, Sahagan BG, Morgan TE, Finch CE, St Laurent G 3rd, Kenny PJ, Wahlestedt C** (2008) Expression of a noncoding RNA is elevated in Alzheimer's disease and drives rapid feed-forward regulation of beta-secretase. *Nat Med* **14**: 723–730
- Fuchs S, Grill E, Meskiene I, Schweighofer A** (2013) Type 2C protein phosphatases in plants. *FEBS J* **280**: 681–693
- Fujii H, Chinnusamy V, Rodrigues A, Rubio S, Antoni R, Park SY, Cutler SR, Sheen J, Rodriguez PL, Zhu JK** (2009) In vitro reconstitution of an abscisic acid signalling pathway. *Nature* **462**: 660–664
- Garcia-Andrade J, Gonzalez B, Gonzalez-Guzman M, Rodriguez PL, Vera P** (2020) The role of ABA in plant immunity is mediated through the PYR1 receptor. *Int J Mol Sci* **21**:5852
- Hao Q, Yin P, Li W, Wang L, Yan C, Lin Z, Wu JZ, Wang J, Yan SF, Yan N** (2011) The molecular basis of ABA-independent inhibition of PP2Cs by a subclass of PYL proteins. *Mol Cell* **42**: 662–672
- Harris CJ, Scheibe M, Wongpalee SP, Liu WL, Cornett EM, Vaughan RM, Li XQ, Chen W, Xue Y, Zhong ZH, et al.** (2018) A DNA methylation reader complex that enhances gene transcription. *Science* **362**: 1182– +
- Katiyar-Agarwal S, Morgan R, Dahlbeck D, Borsani O, Villegas A Jr, Zhu JK, Staskawicz BJ, Jin H** (2006) A pathogen-inducible endogenous siRNA in plant immunity. *Proc Natl Acad Sci USA* **103**: 18002–18007
- Kerk D, Templeton G, Moorhead GB** (2008) Evolutionary radiation pattern of novel protein phosphatases revealed by analysis of protein data from the completely sequenced genomes of humans, green algae, and higher plants. *Plant Physiol* **146**: 351–367
- Kindgren P, Ard R, Ivanov M, Marquardt S** (2018) Transcriptional read-through of the long non-coding RNA SVALKKA governs plant cold acclimation. *Nat Commun* **9**: 4561
- Lapidot M, Pilpel Y** (2006) Genome-wide natural antisense transcription: coupling its regulation to its different regulatory mechanisms. *EMBO Rep* **7**: 1216–1222
- Li H, Handsaker B, Wysoker A, Fennell T, Ruan J, Homer N, Marth G, Abecasis G, Durbin R, Proc GPD** (2009) The sequence alignment/map format and SAMtools. *Bioinformatics* **25**: 2078–2079
- Li Q, Wang B, Yu JP, Dou DL** (2021) Pathogen-informed breeding for crop disease resistance. *J Integr Plant Biol* **63**: 305–311
- Li Q, Ai G, Shen D, Zou F, Wang J, Bai T, Chen Y, Li S, Zhang M, Jing M, et al.** (2019) A *Phytophthora capsici* effector targets ACD11 binding partners that regulate ROS-mediated defense response in Arabidopsis. *Mol Plant* **12**: 565–581
- Li Y, Li X, Yang J, He Y** (2020) Natural antisense transcripts of MIR398 genes suppress microR398 processing and attenuate plant thermotolerance. *Nat Commun* **11**: 5351
- Lillo C, Kataya AR, Heidari B, Creighton MT, Nemie-Feyissa D, Ginbot Z, Jonassen EM** (2014) Protein phosphatases PP2A, PP4 and PP6: mediators and regulators in development and responses to environmental cues. *Plant Cell Environ* **37**: 2631–2648
- Liu J, Wang H, Chua NH** (2015) Long noncoding RNA transcriptome of plants. *Plant Biotechnol J* **13**: 319–328
- Lorkovic ZJ** (2009) Role of plant RNA-binding proteins in development, stress response and genome organization. *Trends Plant Sci* **14**: 229–236
- Lorkovic ZJ, Barta A** (2002) Genome analysis: RNA recognition motif (RRM) and K homology (KH) domain RNA-binding proteins from the flowering plant *Arabidopsis thaliana*. *Nucleic Acids Res* **30**: 623–635
- Ma L, Cheng K, Li J, Deng Z, Zhang C, Zhu H** (2021) Roles of plant glycine-rich RNA-binding proteins in development and stress responses. *Int J Mol Sci* **22**:5849
- Mine A, Berens ML, Nobori T, Anver S, Fukumoto K, Winkelmueller TM, Takeda A, Becker D, Tsuda K** (2017) Pathogen exploitation of an abscisic acid- and jasmonate-inducible MAPK phosphatase and its interception by Arabidopsis immunity. *Proc Natl Acad Sci USA* **114**: 7456–7461
- Park SY, Fung P, Nishimura N, Jensen DR, Fujii H, Zhao Y, Lumba S, Santiago J, Rodrigues A, Chow TF, et al.** (2009) Abscisic acid inhibits type 2C protein phosphatases via the PYR/PYL family of START proteins. *Science* **324**: 1068–1071
- Pavan S, Jacobsen E, Visser RGF, Bai YL** (2010) Loss of susceptibility as a novel breeding strategy for durable and broad-spectrum resistance. *Mol Breed* **25**: 1–12
- Pertea M, Kim D, Pertea GM, Leek JT, Salzberg SL** (2016) Transcript-level expression analysis of RNA-seq experiments with HISAT, StringTie and Ballgown. *Nature Protoc* **11**: 1650–1667
- Robinson JT, Thorvaldsdottir H, Winckler W, Guttman M, Lander ES, Getz G, Mesirov JP** (2011) Integrative genomics viewer. *Nat Biotechnol* **29**: 24–26
- Schwab R, Ossowski S, Riester M, Warthmann N, Weigel D** (2006) Highly specific gene silencing by artificial microRNAs in Arabidopsis. *Plant Cell* **18**: 1121–1133
- Schweighofer A, Hirt H, Meskiene L** (2004) Plant PP2C phosphatases: emerging functions in stress signaling. *Trends Plant Sci* **9**: 236–243
- Schweighofer A, Kazanaviciute V, Scheikl E, Teige M, Doczi R, Hirt H, Schwanninger M, Kant M, Schuurink R, Mauch F, et al.** (2007) The PP2C-type phosphatase AP2C1, which negatively regulates MPK4 and MPK6, modulates innate immunity, jasmonic acid, and ethylene levels in Arabidopsis. *Plant Cell* **19**: 2213–2224
- Seo JS, Diloknawarit P, Park BS, Chua NH** (2019) ELF18-INDUCED LONG NONCODING RNA 1 evicts fibrillarlin from mediator subunit to enhance PATHOGENESIS-RELATED GENE 1 (PR1) expression. *New Phytol* **221**: 2067–2079
- Seo JS, Sun HX, Park BS, Huang CH, Yeh SD, Jung C, Chua NH** (2017) ELF18-INDUCED LONG-NONCODING RNA associates with mediator to enhance expression of innate immune response genes in Arabidopsis. *Plant cell* **29**: 1024–1038
- Shen SH, Park JW, Lu ZX, Lin L, Henry MD, Wu YN, Zhou Q, Xing Y** (2014) rMATs: Robust and flexible detection of differential alternative splicing from replicate RNA-Seq data. *Proc Natl Acad Sci USA* **111**: E5593–E5601.
- Shi YG** (2009) Serine/threonine phosphatases: mechanism through structure. *Cell* **139**: 468–484
- Silverman IM, Li F, Gregory BD** (2013) Genomic era analyses of RNA secondary structure and RNA-binding proteins reveal their significance to post-transcriptional regulation in plants. *Plant Sci* **205–206**: 55–62
- Singh A, Pandey A, Srivastava AK, Tran LS, Pandey GK** (2016) Plant protein phosphatases 2C: from genomic diversity to functional multiplicity and importance in stress management. *Crit Rev Biotechnol* **36**: 1023–1035
- Sun YD, Li L, Macho AP, Han ZF, Hu ZH, Zipfel C, Zhou JM, Chai JJ** (2013) Structural basis for flg22-induced activation of the Arabidopsis FLS2-BAK1 immune complex. *Science* **342**: 624–628
- Tian L, Chou HL, Zhang L, Hwang SK, Starkenburg SR, Doroshenko KA, Kumamaru T, Okita TW** (2018) RNA-binding protein RBP-P is required for glutelin and prolamine mRNA localization in rice endosperm cells. *Plant Cell* **30**: 2529–2552
- Tischer SV, Wunschel C, Papacek M, Kleigrew K, Hofmann T, Christmann A, Grill E** (2017) Combinatorial interaction network of abscisic acid receptors and coreceptors from *Arabidopsis thaliana*. *Proc Natl Acad Sci USA* **114**: 10280–10285
- Wang JY, Yu WG, Yang YW, Li X, Chen TZ, Liu TL, Ma N, Yang X, Liu RY, Zhang BL** (2015) Genome-wide analysis of tomato long non-coding RNAs and identification as endogenous target mimic for microRNA in response to TYLCV infection. *Sci Rep* **5**:16946
- Wang Y, Cheng X, Shan Q, Zhang Y, Liu J, Gao C, Qiu JL** (2014) Simultaneous editing of three homoeoalleles in hexaploid bread

- wheat confers heritable resistance to powdery mildew. *Nat Biotechnol* **32**: 947–951
- Wierzbicki AT, Blevins T, Swiezewski S** (2021). Long noncoding RNAs in plants. *Annu Rev Plant Biol* **72**: 245–271
- Wu Z, Fang XF, Zhu DL, Deati C** (2020) Autonomous pathway: FLOWERING LOCUS C repression through an antisense-mediated chromatin-silencing mechanism. *Plant Physiol* **182**: 27–37
- Yang YW, Liu TL, Shen DY, Wang JY, Ling XT, Hu ZZ, Chen TZ, Hu JL, Huang JY, Yu WG, et al.** (2019) Tomato yellow leaf curl virus intergenic siRNAs target a host long noncoding RNA to modulate disease symptoms. *PLoS Pathog* **15**: e1007534
- Zhai K, Deng Y, Liang D, Tang J, Liu J, Yan B, Yin X, Lin H, Chen F, Yang D, et al.** (2019) RRM transcription factors interact with NLRs and regulate broad-spectrum blast resistance in rice. *Mol Cell* **74**: 996–1009 e1007
- Zhang M, Su J, Zhang Y, Xu J, Zhang S** (2018a) Conveying endogenous and exogenous signals: MAPK cascades in plant growth and defense. *Curr Opin Plant Biol* **45**: 1–10
- Zhang M, Chiang YH, Toruno TY, Lee D, Ma M, Liang X, Lal NK, Lemos M, Lu YJ, Ma S, et al.** (2018b) The MAP4 kinase SIK1 ensures robust extracellular ROS burst and antibacterial immunity in plants. *Cell Host Microbe* **24**: 379–391 e375
- Zhang X, Ai G, Wang XD, Peng H, Yin ZY, Dou DL** (2020) Genome-wide identification and molecular evolution analysis of BPA genes in green plants. *Phytopathol Res* **2**:6
- Zhang YC, Liao JY, Li ZY, Yu Y, Zhang JP, Li QF, Qu LH, Shu WS, Chen YQ** (2014) Genome-wide screening and functional analysis identify a large number of long noncoding RNAs involved in the sexual reproduction of rice. *Genome Biol* **15**:512
- Zhao J, Zhao L, Zhang M, Zafar SA, Fang J, Li M, Zhang W, Li X** (2017) Arabidopsis E3 ubiquitin ligases PUB22 and PUB23 negatively regulate drought tolerance by targeting ABA receptor PYL9 for degradation. *Int J Mol Sci* **18**:1841
- Zhao X, Li J, Lian B, Gu H, Li Y, Qi Y** (2018) Global identification of Arabidopsis lncRNAs reveals the regulation of MAF4 by a natural antisense RNA. *Nat Commun* **9**: 5056